

16TH INTERNATIONAL CONFERENCE on Communications, Electromagnetics and Medical Applications (CEMA'22)

Sofia, Bulgaria
20th October, 2022



Organized by:
Faculty of Telecommunications of TU-Sofia, Bulgaria



NATIONAL
TECHNICAL UNIVERSITY
OF ATHENS,
GREECE



SCHOOL OF
ELECTRICAL AND
COMPUTER ENGINEERING



PROCEEDINGS

OF 16TH INTERNATIONAL CONFERENCE ON
COMMUNICATIONS, ELECTROMAGNETICS AND MEDICAL
APPLICATIONS (CEMA'22)



Organized by:



FACULTY OF TELECOMMUNICATIONS
TECHNICAL UNIVERSITY OF SOFIA, BULGARIA

NATIONAL TECHNICAL UNIVERSITY OF ATHENS, GREECE,
SCHOOL OF ELECTRICAL AND COMPUTER ENGINEERING

NATIONAL TECHNICAL
UNIVERSITY OF ATHENS,
GREECE



SCHOOL OF ELECTRICAL
AND COMPUTER
ENGINEERING

Sofia, Bulgaria
20st October, 2022

KING 2001, Sofia

Edited by Prof. Dr. Eng. **Dimiter Tz. Dimitrov**

All rights reserved. This book, or parts there of, may not be reproduced in any form or by any means, electronic or mechanical, including photocopying or any information storage and the retrieval system now known or to be invented without written permission from the Publisher.

ISSN: 1314-2100

SCOPUS Indexing

<http://suggestor.step.scopus.com/progressTracker>, ID: 6B4F77263D276412.

Printed in Bulgaria
KING 2001, Sofia



P. Frangos



D. Dimitrov



K. Dimitrov

Dear Colleagues,

It is our privilege to thank all of you for your contributions submitted at 16th regular International Conference on 'Communication, Electromagnetic and Medical Applications' CEMA'22. This is a conference which should help future collaboration in the area of engineering, especially in the area of communication technologies and medical applications. This is an important scientific event not only in Balkan region, but in Europe, also. The International Conference on Communication, Electromagnetism and Medical Applications CEMA'22 is dedicated to all essential aspects of the development of global information and communication technologies, and their impact in medicine, as well. The objective of Conference is to bring together lecturers, researchers and practitioners from different countries, working on the field of communication, electromagnetism, medical applications and computer simulation of electromagnetic field, in order to exchange information and bring new contribution to this important field of engineering design and application in medicine. The Conference will bring you the latest ideas and development of the tools for the above mentioned scientific areas directly from their inventors. The objective of the Conference is also to bring together the academic community, researchers and practitioners working in the field of Communication, Electromagnetic and Medical Applications, not only from all over Europe, but also from America and Asia, in order to exchange information and present new scientific and technical contributions.

Many well known scientists took part in conference preparation as members of International Scientific Committee or/and as reviewers of submitted papers. We would like to thank all of them for their efforts, for their suggestions and advices.

On behalf of the International Scientific Committee, we would like to wish you successful presentations of your papers, successful discussions and new collaborations for your future scientific investigations.

Engineering and medicine should provide high level of living for all people.

D. Dimitrov
Conference Chairman

P. Frangos
Conference Vice Chairman

K. Dimitrov
Conference Vice Chairman

INTERNATIONAL SCIENTIFIC COMMITTEE

Chairman:

D. TZ. DIMITROV, Technical University of Sofia, Bulgaria

Vice Chairmen:

P. FRANGOS, National Technical University of Athens, Greece

K. L. DIMITROV, Technical University of Sofia, Bulgaria

Members

N. AMPILOVA,	University of Petersburg, Russia
T. AVOYAGI,	Tokyo Institute of Technology, Japan
A. BEKJARSKY,	Technical University of Sofia, Bulgaria
E. BOEMO,	University Autnoma, Barcelona, Spain
R. BRUZGIENE,	Kaunas University of Technology, Lithuania
N. DIB,	Jordan University of Science and Technology, Aman, Jordan
V. DUMBRAVA,	Kaunas University of Technology, Litvania
N. ESCUDEIRO,	ISEP, Porto, Portugal
E. GAGO-RIBAS,	University of Oviedo, Spain
V. GEORGIEVA,	Technical University of Sofia, Bulgaria
G. GOUSSETIS,	Heriot - Watt University, United Kingdom
S. V.HOEYE,	University of Oviedo, Spain
I. ILIEV,	Technical University of Sofia, Bulgaria
F. KLETT,	Franhofer Institute, Ilmenau, Germany
G. KLIROS,	Hellenic Air-Force Academy, Athens, Greece
V. KUKENSKA,	Technical University of Gabrovo, Bulgaria
L. LUBIH,	Technical University of Sofia, Bulgaria
G. MALLET,	University "Sophia Antipolis", Nice, France
G. MATSOPOULOS,	National Technical University of Athens, Greece
M. MARTINS,	Academia Militar da Amadora, DCEE, Portugal
M.- J. MORALES-GONZALES,	University of Valladolid, Spain
L. NARBUTAITE,	Kaunas University of Technology, Lithuania
K. NIKITA,	National Technical University of Athens, Greece
M. NIKOLOVA,	High Naval School, Varna, Bulgaria
A. PANAGOPOULOS,	National Technical University of Athens, Greece
J. PETROVSKA,	Medical University of Sofia, Bulgaria
H. ROTH,	University of Siegen, Germany
S. SAUTBEKOV,	Euroasian University, Astana, Kazakhstan
A. SAVOV,	Medical University of Sofia, Bulgaria
S. SAVOV,	Technical University of Varna, Bulgaria
H.-P. SCHADE,	Technical University of Ilmenau, Germany
I. SOLOVIEV,	University of St. Petersburg, Russia
L. SONG,	Technical University of Harbin, China
G. STAMATAKOS,	National Technical University of Athens, Greece
A. USHEVA,	University of Boston, USA
R. VERDONE,	University of Bologna, Italy

REVIEWERS

BALZANO, Q.	University of Maryland, USA
BEHARI, J.	Jawaharlal Nehru University ,New Delhi, India
BOEMO, E.	Technical University of Madrid, Spain
DIMITROV, D.	Technical University of Sofia, Bulgaria
DONTSHEWA, M.	University of Applied Sciences, Dornbirn, Austria
GOUSSETIS, G.	Heriot - Watt University, United Kingdom
MALLET, G.	University "Sophia Antipolis", Nice, France
PETROVSKA, J.	Medical University of Sofia, Bulgaria
PRATO, F.	University of Western Ontario, Canada
ROTH, H.	University of Siegen, Germany
SAVOV, A.	Medical University of Sofia, Bulgaria
SCHADE, H-P.	Technical University of Ilmenau, Germany
SONG, L.	Technical University of Harbin, China
USHEVA, A.	University of Boston, USA

REGISTRATION

October, 20st, 09h 30min - 16h

The conference registration desk will be on-line at
National Technical University of Athens

CONFERENCE PROGRAM

20st October

OPENING CEREMONY

11h - 11h 30min

The Opening Ceremony will be on-line

SCIENTIFIC PROGRAM

20st October

11h 30min - 13h 30min

On-line presentation and discussions

*Chairman: Prof. P. Frangos, School of Electrical and Computing Engineering,
National Technical University of Athens, Greece*

1. SOME APPROACHES TO FINDING ANALYTICAL FORM OF LIMIT CYCLES

Kostadin Sheiretsky, University of National and World Economy, Faculty of Applied Informatics and Statistics, Sofia, Bulgaria, Svetlin Antonov, Technical University of Sofia, Faculty of telecommunications, Sofia, Bulgaria

2. ON SOME CASES OF USING THE SMALL PARAMETER METHOD FOR FINDING PERIODIC SOLUTIONS

Kostadin Sheiretsky, University of National and World Economy, Faculty of Applied Informatics and Statistics, Sofia, Bulgaria, Svetlin Antonov, Technical University of Sofia, Faculty of telecommunications, Sofia, Bulgaria

3. ON THE INVESTIGATION OF TIME SERIES BY NONLINEAR DYNAMICS METHOD

N. Ampilova, St. Petersburg State University, St. Petersburg, Russia

4. APPLICATION OF MULTIFRACTAL METHODS FOR THE ANALYSIS OF CRYSTAL STRUCTURES

I. Soloviev, St. Petersburg State University, St. Petersburg, Russia

5. REAL-TIME CLASSIFICATION OF FLYING QUADCOPTER AUDIO SIGNALS BY MEL SPECTROGRAMS

Andrey Kadomskij, St. Petersburg State University, St. Petersburg, Russia

6. HAND INFLUENCE ON THE MOBILE PHONE ANTENNAS' MATCHING TO THE FREE SPACE

Tamar Nozadze, Ivane Javakhishvili Tbilisi State University, Laboratory of Applied Electrodynamics and Radio Engineering, Mtvvarisa Kurtsikidze, Samtskhe-Javakheti State University, Veriko Jeladze, Ivane Javakhishvili Tbilisi State University, Laboratory of

Applied Electrodynamics and Radio Engineering, Giorgi Ghvedashvili, Ivane Javakishvili Tbilisi State University, Laboratory of Applied Electrodynamics and Radio Engineering

7. FPGA BASED EDGE DETECTION: INTEGER SQUARE ROOT ALGORITHM

Dimitre Kromichev, Department of Marketing and International Economic Relations, University of Plovdiv, Bulgaria

8. FPGA BASED EDGE DETECTION: INTEGER INVERSE TANGENT ALGORITHM

Dimitre Kromichev, Department of Marketing and International Economic Relations, University of Plovdiv, Bulgaria

9. DEVELOPMENT OF MODELS FOR SPEECH RECOGNITION AND NATURAL LANGUAGE UNDERSTANDING USING IOT MODULES WITH PARALLEL ARCHITECTURES

Snezhana Pleshkova, Aleksander Bekyarski, Technical University of Sofia, Faculty of Telecommunication, Sofia, Bulgaria

CLOSING CONFERENCE

13h 30min - 14h

CONTACT US:

<http://rcvt.tu-sofia.bg/CEMA/eth.html>

Prof. Dr. Dimiter Dimitrov

Faculty of Telecommunication
Technical University of Sofia
8, Kliment Ohridsky str.
1756 Sofia, Bulgaria
Phone: ++359 2 9652278
Fax: ++359 2 9652278
E-mail: dcd@tu-sofia.bg

Prof. P. Frangos

National Technical University of Athens
School of Electrical and Computer Engineering
9, Iroon Polytechniou Str. ,
157 73 Zografou, Athens, Greece
Phone : 00 30 210 772 3694
Fax : 00 30 210 772 2281
E-mail : pfrangos@central.ntua.gr

TABLE OF CONTENTS

1. SOME APPROACHES TO FINDING ANALYTICAL FORM OF LIMIT CYCLES	1
<i>Kostadin Sheiretsky, Svetlin Antonov</i>	
2. ON SOME CASES OF USING THE SMALL PARAMETER METHOD FOR FINDING PERIODIC SOLUTIONS	5
<i>Kostadin Sheiretsky, Svetlin Antonov</i>	
3. ON THE INVESTIGATION OF TIME SERIES BY NONLINEAR DYNAMICS METHOD	8
<i>N. Ampilova</i>	
4. APPLICATION OF MULTIFRACTAL METHODS FOR THE ANALYSIS OF CRYSTAL STRUCTURES	13
<i>I. Soloviev</i>	
5. REAL-TIME CLASSIFICATION OF FLYING QUADCOPTER AUDIO SIGNALS BY MEL SPECTROGRAMS	18
<i>Andrey Kadomskij</i>	
6. HAND INFLUENCE ON THE MOBILE PHONE ANTENNAS' MATCHING TO THE FREE SPACE	21
<i>Tamar Nozadze, Mtvvarisa Kurtsikidze, Veriko Jeladze, Giorgi Ghvedashvili</i>	
7. FPGA BASED EDGE DETECTION: INTEGER SQUARE ROOT ALGORITHM	25
<i>Dimitre Kromichev</i>	
8. FPGA BASED EDGE DETECTION: INTEGER INVERSE TANGENT ALGORITHM	30
<i>Dimitre Kromichev</i>	
9. DEVELOPMENT OF MODELS FOR SPEECH RECOGNITION AND NATURAL LANGUAGE UNDERSTANDING USING IOT MODULES WITH PARALLEL ARCHITECTURES	35
<i>Snezhana Pleshkova, Aleksander Bekyarski</i>	

SOME APPROACHES TO FINDING ANALYTICAL FORM OF LIMIT CYCLES

Kostadin Sheiretsky

University of National and World Economy, Faculty of Applied Informatics and Statistics, Sofia, Bulgaria
E-mail: sheyretski@unwe.bg

Svetlin Antonov

Technical university of Sofia, Faculty of telecommunications, Sofia
E-mail: svantonov@yahoo.com , ORCID: 0000-0002-1698-8506

Abstract

A variant of the harmonic balance method is presented for finding a solution to limit cycle systems. It is shown how the solution can be constructed using the presence of a small parameter in the equation and in the absence of such a parameter. One way to prove loop stability is considered

1. INTRODUCTION

The change of a system can be traced [1] in phase space – a coordinate system formed by the variables and their velocities, and the qualitative behavior of the solution of the corresponding differential equation describing the system is called a phase portrait.

A closed phase portrait trajectory is called a limit cycle if there exists a tubular neighborhood of the trajectory that contains no other closed trajectories. There are three types of limit cycles: stable – the trajectories wind around the limit cycle on both sides of it, unsustainable – its trajectories spiral away from the limit cycle on both sides of it, and semi-stable – on one side the trajectories wind around the limit cycle, and on the other they move away from him.

2. A METHOD FOR FINDING AN ANALYTICAL FORM OF THE LIMIT CYCLE IN THE PRESENCE OF A SMALL PARAMETER

Let us look for a stationary solution of an equation of the type:

$$\ddot{x} + \omega^2 x + \varepsilon f(x, \dot{x}) = 0. \quad (1)$$

Let us look for the solution of the differential equation (1) in the form [2]:

$$x = x_1 + \beta + x_2 + x_3 + \dots \quad (2)$$

$$x_i = a_i \cos i \psi + b_i \sin i \psi, \psi = k_0 t + \delta_0, \quad (3)$$

where a_i, b_i, k_0, δ_0 and β are constants for $i = 1..n$. In order to obtain an unambiguous decision, we will accept $b_1 = 0$. We impose the condition

$$\begin{aligned} & \sum_{i=1}^n (\ddot{x}_i + (ik_0)^2 x_i) = \\ & = \sum_{i=1}^n [(ik_0)^2 - \omega^2] x_i - \omega^2 \beta - \\ & - \varepsilon f \left(\sum_{i=1}^n x_i + \beta, \sum_{i=1}^n \dot{x}_i \right) = 0. \end{aligned} \quad (4)$$

Let

$$S_1 = \sum_{i=1}^n x_i + \beta, S_2 = \sum_{i=1}^n \dot{x}_i.$$

In general, the sought quantities, decomposed in order by the powers of the small parameter, can be found using the system:

$$(k_0^2 - \omega^2) a_1 = \frac{\varepsilon}{\pi} \int_0^{2\pi} f(S_1, S_2) \cos \psi d\psi, \quad (5)$$

$$\int_0^{2\pi} f(S_1, S_2) \sin \psi d\psi = 0, \quad (6)$$

$$\omega^2 \beta = -\varepsilon \int_0^{2\pi} f(S_1, S_2) d\psi, \quad (7)$$

$$a_j = \frac{\varepsilon}{\pi[(k_0 j)^2 - \omega^2]} \int_0^{2\pi} f(S_1, S_2) \cos j\psi d\psi \quad (8)$$

$$b_j = \frac{\varepsilon}{\pi[(k_0 j)^2 - \omega^2]} \int_0^{2\pi} f(S_1, S_2) \sin j\psi d\psi \quad (9)$$

$$j = 2, 3, \dots, n;$$

Let's look at the van der Pol equation as an example.

$$\ddot{x} + x - \varepsilon(1 - x^2)\dot{x} = 0, \quad (10)$$

where ε is a small parameter. We will look for the solution in the form:

$$x = x_1 + \beta + x_2 + x_3 + \dots, \quad (11)$$

as it must satisfy the condition:

$$\begin{aligned} & \ddot{x}_1 + k_0^2 x_1 + \\ & + \ddot{x}_2 + 4k_0^2 x_2 + \\ & + \ddot{x}_3 + 9k_0^2 x_3 = \\ & = (k_0^2 - 1)x_1 + \\ & + (4k_0^2 - 1)x_2 + \\ & + (9k_0^2 - 1)x_3 - \beta + \\ & + \varepsilon(1 - x_s^2) \frac{d}{dt} x_s = 0, \\ & x_s = x_1 + \beta + x_2 + x_3. \end{aligned} \quad (12)$$

Due to the presence of the first derivative on the right-hand side of the first equality, we will choose x_i as follows:

$$\begin{aligned} x_i &= a_i \cos i\psi + b_i \sin i\psi, \\ \psi &= k_0 t + \delta_0, \\ b_1 &= 0. \\ i &= 1..n. \end{aligned} \quad (13)$$

By substituting in the above equality, after the necessary calculations, it is established that a stationary process is possible at the following values of the quantities:

$$\begin{aligned} k_0 &= 1, a_1 = 2, a_2 = 0, b_2 = 0, a_3 = 0, \\ b_3 &= \varepsilon \frac{a_1^3}{32}, \beta = 0. \end{aligned} \quad (14)$$

3. CONSTRUCTING A SOLUTION BY THE HARMONIC BALANCE METHOD WITHOUT APPARENT DEPENDENCE ON A SMALL PARAMETER

Let's find an approximate solution to the equation.

$$\ddot{x} - \dot{x}(1 - 3x^2 - 2\dot{x}^2) + x = 0. \quad (15)$$

We will look for the solution of equation (15) as a sum of two terms:

$$x = x_1 + x_3. \quad (16)$$

Since preliminary estimates give $a < 1$, this amplitude can be assumed to be a small parameter, a circumstance that we only consider in order to

break the order to $O(a^4)$. We write both terms in the form:

$$\begin{aligned} x_1 &= a \cos \psi, \\ x_3 &= a^3 \mu_1 \sin 3\psi + a^3 \mu_2 \cos 3\psi, \\ \psi &= k_0 t + \gamma. \end{aligned} \quad (17)$$

Where μ_1, μ_2, γ and k_0 are constants to be determined by the harmonic balance method.

We translate the main equation (15) into the form:

$$\begin{aligned} & \ddot{x}_1 + k_0^2 x_1 + \ddot{x}_3 + 9k_0^2 x_3 = \\ & = (k_0^2 - 1)x_1 + (9k_0^2 - 1)x_3 + \\ & + (\dot{x}_1 + \dot{x}_3)[(1 - 3(x_1 + x_3)^2 - \\ & 2(\dot{x}_1 + \dot{x}_3)^2)] = 0. \end{aligned} \quad (18)$$

Equation (18) leads to solving only algebraic equations. Substituting into the equation accordingly, we get:

$$(k_0^2 - 1)a \cos \psi = 0, \quad (19)$$

$$ak_0 \left(1 - \frac{3a^2}{4} - \frac{3a^2 k_0^2}{2}\right) \sin \psi = 0, \quad (20)$$

$$\left[(9k_0^2 - 1)\mu_1 a^3 - 3\mu_2 a^3 - ak_0 \left(-\frac{3a^2}{4} + \frac{a^2 k_0^2}{2}\right)\right] \sin 3\psi = 0 \quad (21)$$

$$\left[(9k_0^2 - 1)\mu_2 a^3 + 3\mu_1 a^3\right] \cos 3\psi = 0. \quad (22)$$

After calculation it is obtained:

$$k_0^2 = 1, a = \frac{2}{3}, \mu_1 = -\frac{2}{73}, \mu_2 = \frac{3}{292}. \quad (23)$$

Due to the fact that the harmonic balance method generally does not use the small parameter concept, the solution can be improved by adding new terms and breaking the order to our chosen harmonic functions, which can easily be done by computer.

4. LIMIT CYCLE STABILITY ANALYSIS

An important role in the study of limit cycles is played by the concept of a positive invariant set - this is a set such that, if we choose an arbitrary point of it as a starting point, then during the further evolution of the system, the trajectory will remain in this set [1].

Let us study systems admitting limit cycles, which generally have the mathematical expression:

$$\ddot{x} + \omega^2 x = F(x, \dot{x}). \quad (24)$$

To investigate the system we will put:

$$x = a(t) \cos \psi, \psi = \omega t + \delta(t). \quad (25)$$

We also accept:

$$\begin{aligned} \dot{a} \cos \psi - a \dot{\delta} \sin \psi &= 0, \\ \dot{x} &= -\omega a \sin \psi. \end{aligned} \quad (26)$$

By substituting into equation (25), the system is reached:

$$\begin{aligned} \dot{a} &= -\frac{1}{\omega} F(a \cos \psi, -\omega a \sin \psi) \sin \psi, \\ \dot{\delta} &= -\frac{1}{a\omega} F(a \cos \psi, -\omega a \sin \psi) \cos \psi. \end{aligned} \quad (27)$$

If a limit cycle exists, it will be a closed curve with equation:

$$F(a \cos \psi, -\omega a \sin \psi) = 0. \quad (28)$$

This fact can become clearer if we consider the following statement derived on the basis of a statement presented in [3].

Let $F(a \cos \psi, -\omega a \sin \psi)$ be a continuous function of its variables. If there exist two real positive numbers a_1 and a_2 such that $a_1 < a_2$ and the conditions are met:

$$\begin{aligned} -F(a \cos \psi, -\omega a \sin \psi) &> 0, \text{ if } a < a_1 \\ -F(a \cos \psi, -\omega a \sin \psi) &< 0, \text{ if } a > a_2 \end{aligned}$$

for any value of ψ , there exists a positive invariant set $M = \{x | a_1 < a < a_2\}$.

The condition 1 shows that: $\dot{a} > 0$ for $a < a_1$, and the condition 2 shows respectively, that: $\dot{a} < 0$ for $a > a_2$ and since F is continuous with respect to a , it will exist $a^*(\psi)$, such that $F(a^*(\psi) \cos \psi, -\omega a^*(\psi) \sin \psi) = 0$, for any fixed ψ . The fact is obvious that for amplitude values $a_1 < a < a_2$, the phase trajectory "winds" on the closed curve described by the equation

$$F(a^*(\psi) \cos \psi, -\omega a^*(\psi) \sin \psi) = 0$$

when $\psi \in \left[0, \frac{2\pi}{\omega}\right]$.

As a consequence, the fact can be established that at $a_1 > a_2$ the limit cycle will be unstable.

Finding a_1 and a_2 can be done by considering that:

$$\begin{aligned} a_1 &= \min\{a | F(a, \psi) = 0\}; \\ a_2 &= \max\{a | F(a, \psi) = 0\}. \end{aligned} \quad (29)$$

Let's take just an example:

$$\begin{aligned} \dot{x} + x &= \dot{x}(1 - \lambda_1 x^2 - \lambda_2 \dot{x}^2), \\ \lambda_1 &> \lambda_2 > 1. \end{aligned} \quad (30)$$

Taking into account the conditions for finding the limits of the positive invariant set, we arrive at the equations:

$$\begin{aligned} a_1 &= \frac{1}{\sqrt{\max\left\{\frac{\lambda_1 + \lambda_2}{2} + \frac{\lambda_1 - \lambda_2}{2} \cos 2\psi\right\}}}, \\ a_2 &= \frac{1}{\sqrt{\min\left\{\frac{\lambda_1 + \lambda_2}{2} + \frac{\lambda_1 - \lambda_2}{2} \cos 2\psi\right\}}}. \end{aligned} \quad (31)$$

We may take specific values for $\lambda_1 = 3$ and $\lambda_2 = 2$. Then it is easy to define the positive invariant set:

$$M = \left\{x \mid \frac{1}{\sqrt{3}} < a < \frac{1}{\sqrt{2}}\right\}. \quad (32)$$

A result that differs slightly from the estimates of [1]:

$$M = \left\{x \mid \frac{1}{2} < a < \frac{1}{\sqrt{2}}\right\}. \quad (33)$$

Due to the simple structure of the equation, we can immediately write down the equation of the limit cycle:

$$a^*(\psi) = \frac{\sqrt{\frac{2}{\lambda_1 + \lambda_2}}}{\sqrt{1 + \frac{\lambda_1 - \lambda_2}{\lambda_1 + \lambda_2} \cos 2\psi}}. \quad (34)$$

Very rarely can one arrive at an analytical expression for the limit cycle equation. In most cases, it is necessary to use asymptotic methods to find an approximate solution [4, 5, 6, 7]. Such use is in help in the area of Telecommunications, Fluid dynamics and Fire protection analysis.

5. ACKNOWLEDGMENTS

The authors would like to thank the Research and Development Sector at the Technical University of Sofia for the financial support.

References

- [1] Arrowsmith, D. Place, C. Ordinary Differential Equations. A Qualitative Approach with Applications. Chapman and Hall, London, New York 1982.

- [2] O. Blacker, Analysis of Nonlinear Systems [Russian translation], Mir, Moscow, 1969.
- [3] Nemytski V., V. Stepanov. Qualitative Theory of Differential Equations, Princeton University Press 1960.
- [4] Nayfeh, A., Perturbation methods, John Wiley&Sons, Inc., ISBN:9780471399179, Ney York, 2000.
- [5] Bogoliubov N., Mitropolsky A., Asymptotic Methods in the Theory of Non-Linear Oscillations. New York, Gordon and Breach, 1961.
- [6] Andronov A. A., A. A. Vit, S. E. Haikin. Theory of oscillations, Fizmatgiz, M.,1981.
- [7] Sheiretsky, K.G., Antonov, S., Criteria for the existence of a sustainable limit cycle. application of the criteria in the first approximation for the van der pol equation, 56th International Scientific Conference on Information, Communication and Energy Systems and Technologies, ICEST 2021 - Proceedings, ISBN: 978-1-6654-2888-0, DOI: 10.1109/ICEST52640.2021.9483481, 2021, pp. 127-129.

ON SOME CASES OF USING THE SMALL PARAMETER METHOD FOR FINDING PERIODIC SOLUTIONS

Kostadin Sheiretsky

University of National and World Economy, Faculty of Applied Informatics and Statistics, Sofia, Bulgaria
E-mail: sheyretski@unwe.bg

Svetlin Antonov

Technical university of Sofia, Faculty of telecommunications, Sofia
E-mail: svantonov@yahoo.com , ORCID: 0000-0002-1698-8506

Abstract

A modified small parameter method is presented in which the zero-th approximation solution is used to construct the first approximation solution. Simple but practically important differential equations, respectively autonomously and non-autonomously, are considered, showing the application of the method. In the non-autonomous equation, the non-resonant and resonant case are discussed.

1. INTRODUCTION

In the case of nonlinear differential equations, the presence of a small parameter allows to search for a periodic solution in asymptotic order by the powers of this parameter [1]. Usually, such a parameter is embedded in the structure of the equation itself, for example, it can be multiplied before the perturbing term [2, 3]. We will consider a case in which we will look for the decomposition of the solution in order of the degrees of the amplitude [1]. Such an approach can easily be set by a small deviation initial condition for the autonomous differential equation. In the non-autonomous equation, for the non-resonant case, the amplitude will depend on the periodic effect on the oscillator, and if we choose it to have a small amplitude, we will again ensure correctness of the problem. At resonance, the amplitude increases significantly and the asymptotic expansion must be done for a small parameter involved in the structure of the equation [4]. In constructing the asymptotic series itself, we choose the first approximation terms to be a power function of zero approximation. Such use is in help in the area of Telecommunications, Fluid dynamics and Fire protection analysis.

2. AUTONOMOUS CASE

When considering the problem of the movement of the pendulum, for small deviations from the equilibrium position, the formula [3,4] is obtained:

$$\ddot{x} + \omega^2 x - \frac{\omega^2}{6} x^3 = 0. \quad (1)$$

In the equation, ω^2 is a constant quantity. Let's set the initial conditions:

$$x(0) = l, \dot{x}(0) = 0. \quad (2)$$

Since we will be considering small deviations in the equilibrium position, the amplitude l can be used as a small parameter. We do the laying:

$$\Omega t = \tau, \frac{d^2}{dt^2} = \Omega^2 \frac{d^2}{d\tau^2}, \Omega = const \quad (3)$$

and the derivative with respect to variable τ is denoted by ex:

$$\Omega^2 x'' + \omega^2 x - \frac{\omega^2}{6} x^3 = 0. \quad (4)$$

We will look for the solution in the species:

$$x = l\xi_0 + l^3\xi_1 + O(l^5). \quad (5)$$

We also decompose Ω by the powers of the small parameter:

$$\Omega = \omega + l^2\omega_1 + O(l^4). \quad (6)$$

We substitute lines (5) and (6) in the differential equation (4) and arrive at the expressions with the first degree in the small parameter and the third degree in the small parameter, respectively:

$$l: \xi_0'' + \xi_0 = 0, \quad (7)$$

$$l^3: \xi_1'' + \xi_1 = -2\frac{\omega_1}{\omega}\xi_0'' + \frac{1}{6}\xi_0^3. \quad (8)$$

We impose the conditions:

$$\begin{aligned}\xi_0(0) &= 1, \xi_0'(0) = 0; \\ \xi_1(0) &= 0, \xi_1'(0) = 0.\end{aligned}\quad (9)$$

The solution to the first equation can immediately be determined:

$$\xi_0 = \cos \tau. \quad (10)$$

We will look for the solution of equation (8) in the form:

$$\xi_1 = \lambda \xi_0^3 - \lambda \xi_0. \quad (11)$$

We find the second derivative of this function and use that:

$$\xi_0'' = 1 - \xi_0^2, \quad (12)$$

the final result looks like this:

$$\xi_1'' = 6\lambda \xi_0 - 6\lambda \xi_0^3 - 3\lambda \xi_0^3 + \lambda \xi_0. \quad (13)$$

Substituting into the equation gives:

$$\lambda = -\frac{1}{48}, \omega_1 = -\frac{1}{16} \omega. \quad (14)$$

The final solution of the problem in the approximation adopted by us is written in the form:

$$\Omega = \omega \left(1 - \frac{l^2}{16}\right), \quad (15)$$

$$\begin{aligned}x &= l\xi_0 + l^3 \left(-\frac{1}{48} \xi_0^3 + \frac{1}{48} \xi_0\right), \\ \xi_0 &= \cos \Omega t.\end{aligned}\quad (16)$$

3. A NON-AUTONOMOUS CASE

Let us consider the non-autonomous differential equation [1,4]:

$$\ddot{x} + \omega^2 x - \frac{\omega^2}{6} x^3 = F \cos pt. \quad (17)$$

The quantities ω^2 and F are constants.

We will consider only the particular solution when the oscillations are created solely by the perturbing force $F \cos pt$. As in the previous case, we will use the deflection amplitude for a small parameter, this requires the constraint F to be small compared to unity and furthermore the oscillation frequency to be far from the resonance frequencies.

We introduce a new variable:

$$pt = \tau, \quad (18)$$

and substitute in the differential equation (17), noting the derivatives with respect to the new variable with ex:

$$p^2 x'' + \omega^2 x - \frac{\omega^2}{6} x^3 = F \cos \tau. \quad (19)$$

We will look for the solution of (19) in the form:

$$x = q\xi_0 + q^3 \xi_1 + O(q^5). \quad (20)$$

For the function ξ_1 we will take the expression:

$$\xi_1 = \lambda_1 \xi_0^3 - \lambda_2 \xi_0. \quad (21)$$

We substitute expressions (20) and (21) in the differential equation (19) and determine the equations that contain the first power of the amplitude and the third power of the amplitude, respectively. For the first equation we get:

$$qp^2 \xi_0'' + (\omega^2 q - F) \xi_0 = 0. \quad (22)$$

Having accepted that:

$$\xi_0 = \cos \tau. \quad (23)$$

From here it immediately follows that:

$$q = \frac{F}{\omega^2 - p^2}. \quad (24)$$

The values of the unknown parameters we are looking for are also obtained from the equation containing the third degrees of amplitude:

$$6\lambda_1 = \frac{\omega^2}{-9p^2 + \omega^2}, \lambda_2 = -\frac{p^2 \omega^2}{(-9p^2 + \omega^2)(\omega^2 - p^2)}. \quad (25)$$

When we consider the resonant case, we can no longer use the amplitude as a small parameter. Again we consider the case when a small parameter ε appears in the differential equation:

$$p^2 x'' + \omega^2 x - \varepsilon \omega^2 x^3 = \varepsilon F_0 \cos \tau. \quad (26)$$

In equation (26), the derivative is taken with respect to the variable $\tau = pt$. We assume that the frequencies ω and p are close to each other and the relationship between them is carried out by the equation:

$$\omega = p + \varepsilon p_1. \quad (27)$$

We substitute ω in equation (26) and look for x in the form:

$$x = x_0 + \varepsilon x_1, x_1 = \lambda x_0^3. \quad (28)$$

For the zero approximation we get:

$$x_0'' + x_0 = 0. \quad (29)$$

We immediately determine that:

$$x_0 = B \cos \tau. \quad (30)$$

By substituting into the formula for a first approximation, we find the value of λ , as well as the equa-

tion for the relationship between the quantities B , p_1 and F_0 :

$$\lambda = -\frac{1}{8}, \quad (31)$$

$$-\frac{3}{8}p^2B^3 + pp_1B - \frac{F}{2} = 0. \quad (32)$$

4. CONCLUSION

The presented methodology can easily be applied for further approximations. Since approximations to the first or second power of the small parameter are usually used for analytical purposes, the calculations made have a fully justified practical significance [3, 5]. A peculiarity of the presented methodology is that it analytically describes only the stationary process, but not the transient phenomena. This is a characteristic feature of the small parameter method, but nevertheless, for the study of oscillating systems, this method is classical [1]. Numerous applications of this method are the basis of the analytical approach to nonlinear differential equations used in various physical, biological, technical and other models [6, 7]. The authors apply this knowledge especially in Fluid dynamics, Optical and Radio communications, Tele-Medical communications etc. Our approach to this tool is related to the search for a solution as a power function of the zero approximation. The obtained results show that such an approach is justified and can be construct-

ed, the way in which this can be done is also described.

5. ACKNOWLEDGMENTS

The authors would like to thank the Research and Development Sector at the Technical University of Sofia for the financial support.

References

- [1] Andronov A. A., A. A. Vit, S.E.Haikin. Theory of oscillations, Fizmatgiz, M., 1981.
- [2] Bogoliubov N., Mitropolsky A., Asymptotic Methods in the Theory of Non-Linear Oscillations. New York, Gordon and Breach, 1961.
- [3] O. Blacker, Analysis of Nonlinear Systems [Russian translation], Mir, Moscow, 1969.
- [4] Nayfeh, A., Perturbation methods, John Wiley&Sons, Inc., ISBN: 9780471399179, Ney York, 2000.
- [5] Hayashi, C. Nonlinear oscillations in physical systems. McGraw-Hill book company, New York, 1964.
- [6] Zaslavskii, G., R. Sagdeev, Introduction to Nonlinear Physics. Nauka, Moscow, 1988.
- [7] Sheiretsky, K.G., Antonov, S., Formal method for finding asymptotic approximations, 56th International Scientific Conference on Information, Communication and Energy Systems and Technologies, ICEST 2021 - Proceedings, ISBN:978-1-6654-2888-0, 10.1109/ICEST52640.2021.9483465, 2021, pp. 217–219.

ON THE INVESTIGATION OF TIME SERIES BY NONLINEAR DYNAMICS METHOD

N. Ampilova

Saint-Petersburg State University
n.ampilova@spbu.ru

Abstract

Time series are widely used method for representation data of different types. Last 3 decades besides the traditional methods of investigation of time series the approach of nonlinear dynamics – reconstruction of the attractor of the system generating this series – became very popular. It allows calculating correlation dimension of the attractor of the system under study (if it exists) or to establish that the system does not have an attractor.

In this work we apply this method to solve a practical problem to analyze EEG records for revealing the patients with epileptic activity. Additionally we calculate entropy of a signal on amplitude coverage. This approach resulted in separation of 15 records into 2 classes – epileptic activity and other pathologies, and it is in accordance with the expert conclusions.

The implemented program system may be used both for investigations and for educational purpose, and the method may be applied to time series of other types.

1. INTRODUCTION

The notion of time series naturally appears in practice of data processing and statistical analysis. Time series is a ordered sequence of pairs of measured values, one if which is time and other may have a different nature and dimension. Time series are the results of experiments, both real and computational. In particular, the records of various signals are time series. Main problems for time series are *Identification problem* – for given observation data to find parameter of a system which generated this series.

Prognosis problem – for given observation data to predict future values of measured characteristics). The union of traditional methods of investigation of time series with the theory of dynamical systems resulted in occurring of a new approach – the application of nonlinear dynamics methods to the investigation of time series of different nature, namely a reconstruction of the attractor of the system generating this series. [7]. The theoretical substantiation of the reconstruction idea was given by F. Takens in [14]. It is based on the reconstruction of an attractor in a space of a suitable dimension where the attractor does not have self-intersection, i.e embedded. According to Whitney's theorem if an attractor of a system lies in a n -dimensional space then it may be embedded in a space with dimension $2n+1$. Namely this dimension (embedding dimension) is calculated by well-known Grossberg-Procaccia algorithm. This algorithm calculates the correlation dimension of

the attractor, which is the same for the attractor in initial space and the space of embedding. The Grossberg-Procaccia algorithm is a time delay method [2], in which from a given scalar time series one form state vectors with a given time delay. Another method of this class is the method of false neighbors.

Seemingly, nonlinear dynamics methods for the first time were used in medical applications to analyze EEG records [1], [4], [12]. Later on they were applied in geophysics, astrophysics [3], physics, economics for the analysis of financial markets states [15].

The application of reconstruction algorithms for EEG analysis meets many problems, the main of which is non-stationarity of a signal – the state of a patient during recording procedure may change. In this case the record should be divided on several periods in accordance with these states. Besides that, the record length may be insufficient for correct estimation of correlation dimension. The existence of stochastic noise is one more problem.

Research experience in this area shows that the choice of the parameters of reconstruction – time delay and the value of proximity (ε) between state vectors depends on the type of a record and its length. In [8] it was noticed that sometimes the length of time series does not allow the correct choice of ε , and a modified algorithm for the calculation of correlation dimension was proposed. In [9],

[10] the author considered an optimized algorithm for calculation of correlation dimension.

Different algorithms and their implementations, and various variants of the choice of parameters naturally lead to different estimations for correlation dimension. However, researchers note that when solving many practical problems it is the changing of correlation dimension for different types of but not its value is important. In this situation an error in calculation is not essential, and the results of calculations retain their significance.

It was shown in [9] that correlation dimension EEG records for children 4-6 years (recorded in the state of rest) are essentially less than for adults. In [11] the author compared dimensions for 16 channels and revealed the synchronization of α -rhythms in different parts of brain. The authors of [13] obtained the estimation of correlation dimension and separated EEG records of patients with two types of disease.

One of important characteristics of time series is entropy. It may be calculated on amplitude or time coverage. For this purpose Shannon entropy and the class of Renyi entropies are widely used. In [3],[6] the authors applied so called permutation entropy to determine the degree of noise for a time series. The union of nonlinear dynamics methods and entropy characteristics gives a more detailed description of a system under study.

Thus, nonlinear dynamics methods are applied for solving the problems of time series analysis. In this work we present the program system for solving identification problem – reconstruction of the attractor of a system and estimation of correlation dimension of the attractor by a time series generated by the system, and calculation entropy characteristics. The paper has the following structure. In the next section main notions are given, section 3 contains the description of the methods of calculation of correlation dimension and the entropy for amplitude coverage. In the last section the results of experiments for discrete and continuous dynamical systems and EEG records are given.

2. MAIN NOTIONS

Scalar time series is an array on N numbers which are values of a variable $x(t)$ at the moments $t_i = t_0 + \tau(i - 1)$, where τ is called sampling

period [7]. We should make a remark about the choice of parameter τ .

Time series may be obtained as trajectories of discrete dynamical systems or results of numerical integration of continuous ones. In the first case $\tau = 1$, at that time in the last case parameter τ is the step of the numerical method. When recording signal from encephalograph this parameter depends on the recording device. It means that the time between two consecutive values of time series depends on the method of obtaining. As the result, when showing restored attractor we have different representations.

2.1. Takens method

Let $\varphi_t(x)$ be a n -th order dynamical system defined on a compact N -dimensional manifold M , and let we obtained a time series as a result of observation of the system functioning on a coordinate j . Then $\varphi_\tau^j(x)$ is the value of j -th component of $\varphi_t(x)$ at the time τ . If the system has an attractor $A \subset M \subset R^n$, it may be restored in Euclidean space with dimension $2N + 1$.

Define the map $F: M \rightarrow R^{2N+1}$ as the follows $F(x) = (\varphi_0^j(x), \varphi_\tau^j(x), \dots, \varphi_{2N\tau}^j(x))$, where τ is a period of the sample. In what follows we omit the denotation j for simplicity. Construct the vectors from the data of the time series

$$z_0 = (\varphi_0(x), \varphi_1(x), \dots, \varphi_{2N}(x)), \dots, z_i = (\varphi_i(x), \varphi_{i+1}(x), \dots, \varphi_{i+2N}(x)), \dots, z_{K-2N} = (\varphi_{K-2N}(x), \varphi_{K-2N+1}(x), \dots, \varphi_K(x)),$$

where K is the length of the segment of the time series. In other words we construct z_i as a point in the space R^{2N+1} . By the Takens theorem [14] F is embedding M in R^{2N+1} , and it is the generic property. Hence, we have two systems: $\varphi: M \rightarrow M$, and $F: M \rightarrow R^{2N+1}$, which are connected by a nondegenerate change of variables $z = F(x)$. There is the characteristic that is invariant with respect to this change — correlation dimension, and we may obtain the properties of the attractor of the initial system as the properties of its copy in R^{2N+1} .

To determine the dimension of the embedding we follow the algorithm proposed by Grassberg and Procaccia [5]. It proposes to find such N for which there exists a functional dependence between values of the time series. If the system has an attractor

then the points (trajectories) constructed by the time series are close. To estimate the closeness of points we use correlation integral and then calculate correlation dimension of the attractor.

The correlation integral estimates the number of pairs of points (constructed vectors z_i) which are ε -close:

$$C(\varepsilon) = \lim_{K \rightarrow \infty} \frac{1}{K^2} \sum_{n, n_1=1}^K \theta(\varepsilon - \rho(z_n, z_{n_1})), \quad (1)$$

where K is the size the sample and θ is the Heaviside function. The correlation dimension of the attractor is defined as

$$D_c = \lim_{\varepsilon \rightarrow 0} \frac{\log C(\varepsilon)}{\log \varepsilon} \quad (2)$$

and calculated approximately by the least square method as the angular coefficient of the line in coordinates $(\log \varepsilon, \log C(\varepsilon))$.

Thus, by changing the length of vectors z_i (denote it by k) we calculate D_c . This value may reach a stable value or not. In the first case we take the minimal value of k for the dimension of embedding, otherwise we believe that our series is a random noise, not a dynamical system.

The restored attractor is shown in projection to R^2 or R^3 . For the plane one use coordinates $(x(t), x(t+\tau))$, in $R^3 - (x(t), x(t+\tau), x(t+2\tau))$. In this work we use the projection on the plane.

2.2. Entropy on amplitude coverage

Consider the distribution of a signal by amplitude levels. Let x_{max}, x_{min} be maximal and minimal values of the signal respectively, and $\Delta = x_{max} - x_{min}$. Divide Δ on N parts (levels) and define X_i as the number of $x(t)$ belonging to level i .

Define the normed distribution $\{p_i\}$ as $p_i = \frac{X_i}{\sum_i X_i}$ and calculate Shannon entropy $H(N) = -\sum_{i=1}^N p_i \ln p_i$.

3. EXPERIMENTS

The most appropriate way to verify the Takens method is to use dynamical systems having attractors. The length of the obtained series may be taken arbitrary long. We consider examples for 3 types of data.

3.1. Henon map

The transformation is defined on R^2 and given by the formula

$$\begin{aligned} x_{n+1} &= 1 - 1.4x_n^2 + y_n \\ y_{n+1} &= 0.3x_n \end{aligned}$$

It is well known that Henon map has attractor. The results of calculations:

correlation dimension on x coordinate $D_c^x = 1.31$, correlation dimension on y coordinate $D_c^y = 1.25$

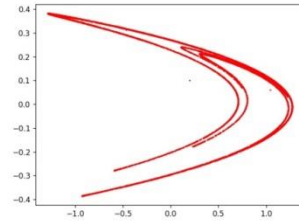


Figure 1. Henon attractor. Initial point (0.2,0.1), 5000 iterations}

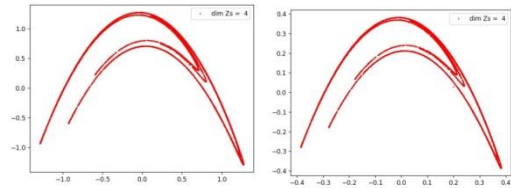


Figure 2. X- and Y- coordinate restored attractors for Henon map

3.2. Predator-prey system

The system is given by the system of differential equations and has the form

$$\begin{aligned} \dot{x} &= (0.7 - 0.65y)x, \\ \dot{y} &= (-0.35 + 2.7x)y. \end{aligned}$$

For numerical integration we use 4th order Runge-Kutta method.

$$D_c^x = 1.05, D_c^y = 1.05.$$

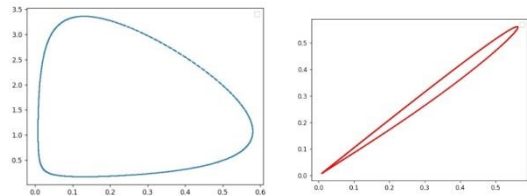


Figure 3. Attractor and x-coordinate restored attractor of predator-prey system. Initial point (0.5,0.55), 5000 iteration, $\tau = 0.1$

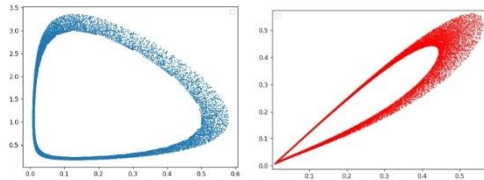


Figure 4. Attractor and x-coordinate restored attractor of predator-prey system Initial point (0.5,0.55), 5000 iteration, $\tau = 0.4$

3.3. EEG records

To calculate D_c we form vectors z_i by length k (starting from $k=2$) and calculate correlation integral for several values of ε by (2). Then we estimate D_c by the least square method. Increase k on 1 and repeat calculations. Compare obtained correlation dimensions. If they are close with a given accuracy δ we believe that the dimension reached a stable value. In this case we take the minimal value of k as the dimension of embedding. If dimensions are not close we again increase k . In the situation when correlation dimension does not reach a limit value we consider the time series is a random noise, not a trace of a dynamical system.

It should be noted that one of main problems when calculating correlation integral is the choice of ε . Due to insufficient length of the time series it is difficult to take this parameter arbitrary, because the situation may occur when there are not pairs of points with such a distance between them. We use the following algorithm:

- take a sequence N_i of parts of a series by increasing length;
- for each N_i calculate distances between vectors z_i, z_j ;
- take the minimal distance and one more as values of ε .

Note that to apply the least square method we need at least two values for ε .

We use 15 EEG records of patients with pathology and separated them into 2 classes – epileptic activity and other pathologies.

Example 1

Series length 514 frequency 80 Hz, time of recording 6.4, the number of channels 16.

Results of calculation

$$D_c = 2.28, H = 1.37 \text{ (using 0 channel)}$$

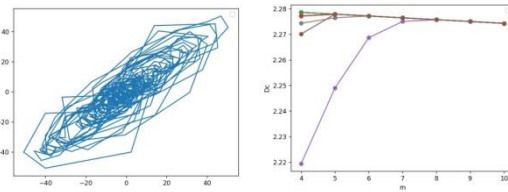


Figure 5. Restored attractor (0 channel) and the graph of stabilization of correlation dimension. Embedding dimension is 8

Example 2

The length of record 2139, frequency 80 Hz, time of recording: 26.73 s, 16 channels

$$D_c \in [3.28 ; 3.44]$$

$$H=2.59 \text{ (using 0 channel)}$$

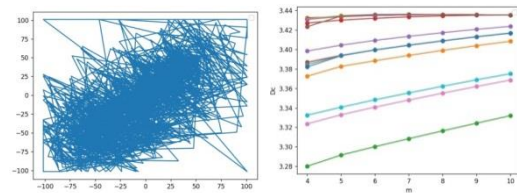


Figure 6. Restored attractor (0 channel) and graphs of correlation dimensions for 16 channels

Summarizing the results for 15 record one may conclude the following. 11 patients were preliminary considered by an expert as having epileptic activity, and 4 patients were diagnosed as having another pathology.

We use the value of interval were correlation dimensions and entropies on amplitude coverage lie. For records corresponding epileptic activity $D_c \in [2.27 ; 2.46]$, and $H \in [0.99 ; 1.37]$. In this case correlation dimension is practically the same for all channels, which means the synchronization process characterizing epilepsy.

For records of other pathology $D_c \in [0.6 ; 1.5] \cup [3.10 ; 3.44]$, $H \in [2.02 ; 2.59]$, and there is no synchronization. Thus, these signs allow the differing epileptic activity from other type of pathology.

4. CONCLUSION

In this work we implemented the investigation of time series by nonlinear dynamics method – reconstruction of attractor and estimation of correlation dimension. The entropy of a time series on amplitude coverage is calculated as an additional characteristic. Continuous and discrete dynamical systems

having attractor and EEG records were considered as test examples.

For dynamical systems the correlation dimension is in accordance with known results, being the calculation is easier than for capacity dimension. For continuous systems the dependence of graphical representation of attractor on the choice of the step of numerical method is illustrated. For EEG records the implemented method allowed the separation of data on 2 classes, which in agreement with expert diagnosis.

These algorithms may be modified and applied to analysis of more complex time series

5. ACKNOWLEDGMENTS

The author thanks V. Lavruhin for computational experiments.

References

- [1] Babloyantz, A. and Destexhe, A, "Low dimensional chaos in an instance of epilepsy". Proc. Nat. Acad. Sci. (USA), 1986, a3: 3513-3517.
- [2] Bezruchko B.P., Smirnov D.A., Mathematical modeling and chaotic time series, 2005, izd. GosUNZ "College", Saratov.(in Russian)
- [3] Chumak O.V., "Entropies and fractals in data analysis", <https://www.researchgate.net/publication/235247584>,2022-04-05 (in Russian)
- [4] Frank, G.W., Lookman, T., Nerengerg, M.A.H., Essex, C., Lemieux, J. and Blume, W. "Chaotic time series analyses of epileptic seizures". Physica D, 1990, 46: 427-438.
- [5] Grassberger P., Procaccia I. "Measuring the strangeness of strange attractors.", Physica D. №1, v.9, 1983. P. 189-208.
- [6] Makarkin S. A., Starodubov A. V., Kalinin Y. A., "Application of permutation entropy in the analysis of chaotic, noise and chaotic-noise series", Journal of technical physics, 2017, v. 87, N. 11, .1712-1717
- [7] Malinezkii G. G., Potapov A. B., Modern problems of nonlinear dynamics,2002, URSS, Moskva (in Russian)
- [8] Mayorov O.Y., Fenchenko V.N., "Calculation of correlation dimension and entropy EEG signals on cluster computer systems", Klinicheskaia informatika I telemedicine,2014,v.10,N.11,10-20 (in Russian)
- [9] Mekler A. A., "Application of nonlinear analysis of dynamical systems for EEG signal processing", Vestnil novih medicinskih tehnologij, 2007,v. Xiv, № 1, 73-77(in Russian)
- [10] Mekler A. A, Program system for the EEG analysis by the dynamical chaos methods, PhD Thesis, SpB, 2006.(in Russian)
- [11] Nikolaeva D. A., "Application of correlation dimension method for analysis of EEG of patients with epilepsy", Differential equations and control processes, №2, 2009, 43-51,<https://diffjournal.spbu.ru/pdf/darina.pdf> (in Russian)
- [12] Roschke J., Aldenhoff J. "The dimensionality of human's electroencephalogram during sleep", Biol. Cybernetics, 1991, 64, p. 307-313.
- [13] Shpitonkov M.I. "Calculation of correlation dimension for physiological time series", Trudi ISA RAN, 2020, v. 702, 75-79 (in Russian)
- [14] Takens F., "On the numerical determination of the dimension of an attractor", In: Dynamical systems and bifurcations (Eds. B.L.J. Braaksma, H. W. Broer and F. Takens). Lect. Notes in Math. 1125, Springer, Heidelberg. 1985.
- [15] Yanovski L. P., Filatov L. A."Analysis of the state of financial markets based on nonlinear dynamics methods", Economical analysis, 2005, 17(50), 5-15 (in Russian)

APPLICATION OF MULTIFRACTAL METHODS FOR THE ANALYSIS OF CRYSTAL STRUCTURES

I. Soloviev

St. Petersburg State University
i.soloviev@spbu.ru

Abstract

We discuss here images of complex structure such as biocrystals, which are very often in applications turn out to be fractals or multifractals. We present 3 types of multifractal spectra, and vector characteristics based on blanket technic for the surface of grey-level function constructed by halftone or monochrome image. Such a set of characteristic describes the image structure quite complete. In this work we apply several different fractal and multifractal methods to analyze images. Our experiments make it obvious that for every class of images at least 2 methods allow obtaining reliable separation of numerical signs. The algorithms for calculation multifractal characteristics are implemented. For each class of images the most appropriate signs were recommended.

1. INTRODUCTION

The study of the properties of various biological substances often uses the technique of obtaining their crystalline forms. In medicine, such methods of crystal growth as adding a substance to a solution of copper chloride, as well as adding a medicinal solution to an oil base, are well known.

In many cases, the properties of the substance under study can be judged by the type of crystal obtained. Methods of analysis and classification of digital images play an important role in the study of the properties of biocrystals. For example, in [1, 2] various approaches to the analysis of images of wheat samples are described, including using artificial neural networks.

Very often in applied problems of biology and medicine, researchers work in conditions of the so-called small sample, when the number of samples is in the tens, whereas most machine learning methods rely on the assumption of samples that differ by orders of magnitude. Therefore, mathematical methods for obtaining fine classification features and the use of expert knowledge are of great importance here. Thus, in [3], the method of multifractal analysis was applied to the study of a set of 60 wheat samples. The obtained characteristics combined with expert assessments allowed us to divide the initial set into 5 classes.

The successful application of multifractal characteristics in the analysis of microscopic images of metal sections [4, 5] and in the study of nanostructures [6] shows that the same methods can be used in the analysis of such complex compounds as biocrystals.

The relevance of this research is due to an increasing number of areas in biological and medical research, where the results of experiments can be recorded by obtaining digital images using modern equipment.

In this work, we apply basic methods of fractal and multifractal analysis of digital images to the study of crystals of biological substrates and drugs, which is used in assessing the quality of biological products and laboratory control of drugs.

As classification features in this paper, we use the characteristics obtained by calculating such indicators as the Minkowski dimension, the Renyi spectrum and the multifractal spectrum determined using a local density function, as well as parametrized spectra.

We show that decomposing an image into disjoint level sets using a local density function allows filtering by selecting the set with the largest capacity dimension. Such sets preserve the main features of the original image, and the use of fractal technic allows for a clearer separation of images.

For images of various classes of biological substrates and drugs, we present the results of experiments.

2. MAIN DEFINITIONS

2.1. Fractal and multifractal characteristics

A natural characteristic of the sets of Euclidean geometry is their topological dimension. It is based on the concept of the multiplicity of the covering

(the smallest number of adjacent elements of the covering -1 , provided that the covering consists of elements having a finite size) and is an integer. Another approach to the notion of dimension was proposed by Hausdorff [7]. For a countable cover with a diameter of elements not exceeding a certain number, we consider a numerical series composed of the diameters of sets raised to a certain power p . The sum of the series is called the Hausdorff measure, it determines the value of p at which the series converges. This value, which is not necessarily an integer, is called the Hausdorff dimension. It is known that for sets of Euclidean geometry, this characteristic coincides with the topological dimension. It turned out that the Hausdorff dimension can also be a characteristic for objects of a more complex structure, namely fractals. Such objects are characterized by fractional dimension. According to the definition proposed by the developer of fractal geometry B. Mandelbrot, a fractal is a set for which Hausdorff dimension is strictly greater than its topological dimension.

Fractal sets have the property of self-similarity. This means that the structure of a part of a fractal set is in some way "similar" to the structure of the whole set. Self-similarity can be strict and statistical. The sets for which the law of their construction is known (the Cantor set, the Serpinsky carpet, etc.) of course have strict self-similarity. Most natural objects with a complex structure can be considered as fractals (or multifractals) with statistical self-similarity.

Sets with strict self-similarity are usually constructed iteratively, from a formal point of view, the process of their construction is endless. When depicting such structures, it is believed that the constructed figure approximates the fractal well and gives a visual representation of its shape, if at a certain step of construction the differences become visually imperceptible.

2.2. Capacity dimension

In practice, calculating the Hausdorff dimension is a time-consuming task, therefore, the class of so-called "box-counting" (capacity) dimensions is used, which are based on the idea of counting the number of coverage elements of linear size ε necessary to cover the set under consideration. When working with fractal sets, we assume that the so-called power law holds, namely, the number of elements of the cover $N(\varepsilon)$ is proportional to the linear size

of the element in some degree $N(\varepsilon) \approx c\varepsilon^{-D}$. This assumption is empirically conditioned.

Usually the capacity dimension of a nonempty bounded set $F \in \mathbb{R}^n$ is defined as follows

$$D = \lim_{\varepsilon \rightarrow 0} \frac{\ln N(\varepsilon)}{-\ln \varepsilon}.$$

An approximate value of the capacity dimension can be obtained, for example, by using the least squares method.

2.3. Minkowski dimension

It should be noted that when analyzing images of fractal sets, the capacity dimension is determined only for black-and-white images.

To calculate the fractal dimension of the sets represented by halftone (gray-scale) images, we can use the Minkowski dimension. It is based on the so-called blanket technic and its calculation does not use a coverage.

A detailed description of this method can be found in [7, 8], so we will provide here only the information necessary to describe the algorithm for its implementation.

Let $F = \{X_{ij}, i = 0, 1, \dots, K, j = 0, 1, \dots, L\}$ be a gray-scale image and X_{ij} be the gray level of the (i, j) -th pixel. This is a gray-level surface for the image, which can be viewed as a fractal for a certain measure range.

Let $F \subset \mathbb{R}^n$. Then δ -parallel body F_δ is a set of points distant from F by no more than δ :

$$F_\delta = \{x \in \mathbb{R}^n : |x - y| \leq \delta, y \in F\}$$

and we say, that $Vol(F_\delta)$ — n -dimensional volume of F_δ .

If for some constant s at $\delta \rightarrow 0$ the limit $Vol(F_\delta)/\delta^{n-D}$ is positive and bounded, then the number D is called the Minkowski dimension of the set F .

We build blankets u_δ, b_δ for a gray level surface as follows

$$\begin{aligned} u_\delta(i, j) &= \\ & \max\{u_{\delta-1}(i, j) + \\ & 1, \max_{|(m,n)-(i,j)| \leq 1} u_{\delta-1}(m, n)\} \\ b_\delta(i, j) &= \\ & \min\{b_{\delta-1}(i, j) - \\ & 1, \min_{|(m,n)-(i,j)| \leq 1} u_{\delta-1}(m, n)\} \end{aligned}$$

$$u_0(i, j) = b_0(i, j) = X_{ij}$$

A point $F(x, y)$ is included in a δ -parallel body if $b_\delta(i, j) < F(x, y) < u_\delta(i, j)$. The definition of a blanket is based on the fact that the blanket for a surface of radius δ includes all the points of the blanket for a surface of radius $\delta - 1$ together with the points that are at the distance of 1 from this blanket.

The volume of a δ -parallel body is calculated by u_δ and b_δ :

$$Vol(F_\delta) = \sum_{i,j} (u_\delta(i, j) - b_\delta(i, j)).$$

The surface area is calculated using one of two formulas

$$A_\delta = \frac{Vol_\delta}{2\delta}$$

$$A_\delta = \frac{Vol_\delta - Vol_{\delta-1}}{2}.$$

Minkovsky dimension is defined as

$$D \approx 2 - \frac{\ln A_\delta}{\ln \delta}$$

To obtain the image characteristics, we use a vector $((\ln \delta, \ln A_\delta))$, the size of which is determined by the number of different values of δ .

2.4. Rényi spectra

Consider the set $M \subset R^n$, and its partition into $N(\varepsilon)$ cells with side (or volume) ε . We define the probability measure $p(\varepsilon) = \{p_i(\varepsilon)\}$, $i = 1, \dots, N(\varepsilon)$, $\sum_{i=1}^{N(\varepsilon)} p_i(\varepsilon) = 1$. Also consider the generalized statistical sum (or the sum of the moments of the measure) [9]

$$S(q, \varepsilon) = \sum_{i=1}^{N(\varepsilon)} p_i^q(\varepsilon), q \in R \quad (1)$$

As usual we assume that the power law holds

$$p_i(\varepsilon) \sim \varepsilon^{\alpha_i} \quad (2)$$

We also assume that the statistical sum itself also follows the power law:

$$S(q, \varepsilon) \sim \varepsilon^{\tau(q)} \quad (3)$$

where $\tau(q)$ is a function of class C^1 .

The symbol \sim in (2) and (3) is understood as follows:

$$\alpha_i = \lim_{\varepsilon \rightarrow 0} \frac{\ln p_i(\varepsilon)}{\ln \varepsilon}, \tau(q) = \lim_{\varepsilon \rightarrow 0} \frac{\ln S(q, \varepsilon)}{\ln \varepsilon} \quad (4)$$

Under these assumptions, the characteristic of a set with a complex structure is a set of generalized Rényi dimensions:

$$D_q = \lim_{\varepsilon \rightarrow 0} \frac{1}{q-1} \frac{\ln S(q, \varepsilon)}{\ln \varepsilon} \quad (5)$$

2.5. Parameterized spectra

A multifractal set can be represented as a set of fractal subsets, each of which has its own fractal dimension. A multifractal spectrum is a set of dimensions of these subsets. Multifractal spectrum is a set of subsets, each of them is the union of covering elements having close values of exponents α_i in (4).

In this sense Rényi spectrum is not multifractal one, because it shows the changing of initial measure when parameter q changes. But one may go from Rényi spectrum to multifractal one by using parametrized spectra [10].

Let M be a set and $\{M_i\}$ be its partition on $N(\varepsilon)$ cells by size ε . Consider a normed measure $\{p_i(\varepsilon)\}$ on $\{M_i\}$ and construct a sequence of measures $\mu(q, \varepsilon) = \{\mu_i(q, \varepsilon)\}$, where

$$\mu_i(q, \varepsilon) = \frac{p_i^q(\varepsilon)}{\sum_{i=1}^{N(\varepsilon)} p_i^q(\varepsilon)}.$$

Define the average $\alpha(q)$ of exponents α_i by a chosen measure

$$\alpha(q) = \lim_{\varepsilon \rightarrow 0} \frac{\sum_{i=1}^N \ln p_i(\varepsilon) \mu_i(q, \varepsilon)}{\ln \varepsilon}$$

For every measure $\mu(q, \varepsilon)$ calculate information dimension $f(q)$ of its support

$$f(q) = \lim_{\varepsilon \rightarrow 0} \frac{\sum_{i=1}^N \mu_i(q, \varepsilon) \ln \mu_i(q, \varepsilon)}{\ln \varepsilon}$$

Excluding parameter q we obtain multifractal spectra $(\alpha, f(\alpha))$.

2.6. Local density function

This method was proposed in [11]. Consider an image I in R^2 and denote the square with center x and radius r (half of the side length) by $B(x, r)$. Denote the measure of pixel intensities by μ .

Assume that

$$\mu(B(x, r)) = kr^{d(x)}(x), \quad (6)$$

where $d(x)$ — local density function and k is a constant.

Consider (6) for r small enough, then it follows

$$d(x) = \lim_{r \rightarrow 0} \frac{\log \mu(B(x, r))}{\log r}$$

The function $d(x)$ characterizes the degree of heterogeneity of the pixel intensities distribution in a neighbour of x . The set of points x with local density α forms the level set

$E_\alpha = \{x \in I: d(x) = \alpha\}$. In practice we calculate $\alpha_{min}, \alpha_{max}$, $\alpha \in [\alpha_{min}, \alpha_{max}]$ and form the sets

$$E(\alpha, \varepsilon) = \{x \in I: d(x) \in [\alpha, \alpha + \varepsilon]\},$$

where ε is a parameter.

We obtain a set of binary images. Obviously, this parameter controls the number of level sets and allows the separation of the image on nonintersecting level sets, and the procedure of separation is a kind of filtration.

Then we calculate capacity dimensions for level sets and obtain multifractal spectrum $f(\alpha)$.

3. EXPERIMENTS

3.1. The effect of cyna

The effect of Cyna 6 on biosubstrates was studied. The images from 2 classes (each contains 5 images) were analyzed by the methods described.

The results are shown below.

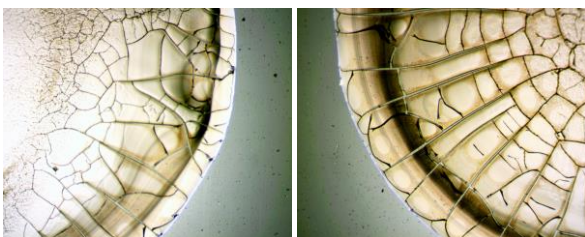


Figure 1. Biosubstrate without correction (left) and after correction (right) .

Graphs are given below. All the calculated features show the separation.

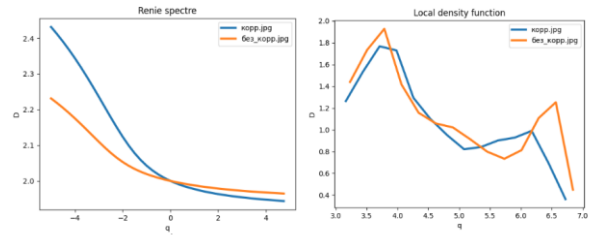


Figure 2. Renyi spectra and multifractal spectra by local density function

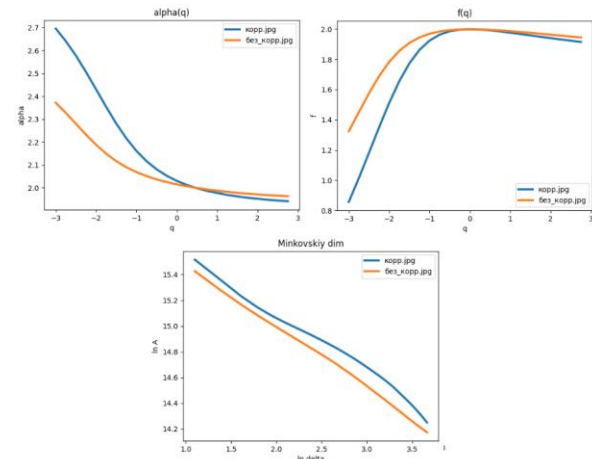


Figure 3. Parametrized spectra and graphs of characteristic vectors

3.2. Crystals of drugs

3 types of crystals of drugs (medical solution is added to oil, crystals are formed on the boundary of matters).

Images are obtained by microscope, every class contains 7-8 images.

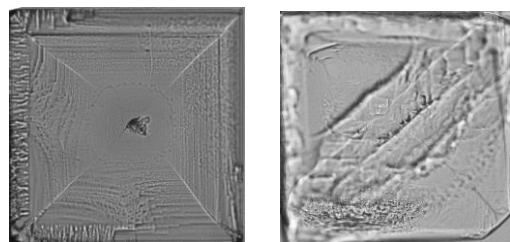


Figure 4. Class 1 (left) and class 2(right)

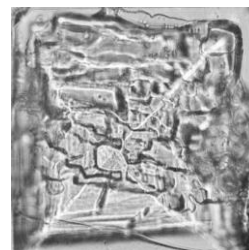


Figure 5. Class 3

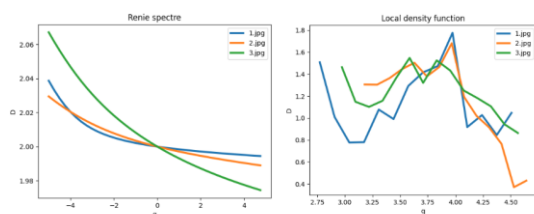


Figure 6. Renyi spectra and multifractal spectra by local density function

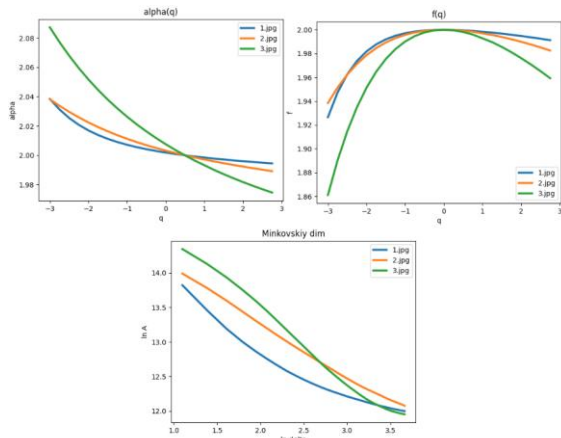


Figure 7. Parametrized spectra and graphs of characteristic vectors

4. CONCLUSION

As a rule, researchers work with images biomedical preparations under conditions of so called small sample — the number of images is estimated in tens, not thousands. It is expert knowledge that has a decisive meaning. However, the practical experience shows that a description of images in terms of numerical characteristics is useful addition to visual perception. Any description of an image structure may be thought as a formalization of expert knowledge. In this work we demonstrate the results of application of several fractal and multifractal methods to analyze images of crystals of drugs. The experiments showed that for every class of images at least 2 methods allow obtaining reliable separation of numerical signs.

ACKNOWLEDGMENTS

The author thanks I. Demidov for his significant help in organizing and performing the necessary experiments.

References

- [1] Khoshroo A. Classification of Wheat Cultivars Using Image Processing and Artificial Neural Networks / A. Khoshroo, A. Arefi // Agricultural Communications, . — 2014. — № 2 (1). — C.17-22.
- [2] P. Sadeghi-Tehran. DeepCount: In-Field Automatic Quantification of Wheat Spikes Using Simple Linear Iterative Clustering and Deep Convolutional Neural Networks, *Frontiers in Plant Science*. 2019, v. 10. <https://doi.org/10.3389/fpls.2019.01176>.
- [3] Murenin I., Ampilova N. Analysis of Wheat Samples Using the Calculation of Multifractal Spectrum , *Computer Tools in Education*, 2021, № 1,p. 5-20.
- [4] Vstovsky G.V. Elements of information physics M, MGIU 2002. (in Russian)
- [5] Bortnikov A.Y., Minakova N. N. Texturno-fraktalnii analiz mikroskopicheskikh srezov obraztsov rompozisionnih materialov zapolnennih technicheskim uglerodom, *Izv TPU*, 2006. №6.(in Russian).
- [6] Polischuk S.V., Petrov K.A. Otsenka fraktalnih svoystv nanostruktur po mikroskopicheskim izobrazheniyam, *MNIG*, 2022. №2-1 (116).(in Russian)
- [7] Falconer, K. J. *Fractal geometry* / K. J. Falconer. — Chichester : Wiley,1990.
- [8] Tang, Y. Y. Modified fractal signature (MFS): a new approach to document analysis for automatic knowledge acquisition Y. Tang, C. Y. Suen // *IEEE Transactions on Knowledge and Data Engineering*,1997, 9, № 5,p. 747-762.
- [9] Kuznetsov S.P. *Dynamical chaos*, M, *Izd.fiz-mat lit.*,2001
- [10] Chhabra A. B, Direct determination of the $f(\alpha)$ singularity spectrum and its application to fully developed turbulence , *Physical Review A*,1989,v. 40, № 9. p. 5284-5294.
- [11] Y. Xu, H. Ji, C. Fermüller , Viewpoint Invariant Texture Description Using Fractal Analysis, *International Journal of Computer Vision*, 2009,v. 83, № 1,p. 85-100.

REAL-TIME CLASSIFICATION OF FLYING QUADCOPTER AUDIO SIGNALS BY MEL SPECTROGRAMS

Andrey Kadomskij

St. Petersburg State University
st099001@student.spbu.ru

Abstract

In the article we suggest a method for detection of quadcopters by sound by means of Mel Spectrograms. For the experiment, audio recordings of both flying quadcopters signals and noises were collected. The experiments were performed by means of spectrograms with 2 classes, Mel Spectrograms with 2 classes and Mel Spectrograms with 4 classes. The method has proved to be effective at testing and can be used for quadcopter real-time detection software.

1. INTRODUCTION

To classify quadcopters various techniques are applied, such as

- Visual analysis. Analysis of camera image for the search of a quadcopter. This method is significantly dependable on the camera scope. If the quadcopter is at certain distance, it will be difficult to differentiate it from other small objects (for example birds). The efficiency is also reduced in heavy weather conditions (fog, rain, snow). [1]
- Radar. Due to the narrow scope radars cannot insure efficient quadcopter detection. [2]
- Sound analysis. The interest to the sound detection of quadcopters has appeared recently, and only few researches concern this theme. [3]

In this work the sound analysis is used for a classification.

The paper [3] analyses the frequencies of quadcopter motor and rotors. This method does not allow detecting other quadcopters, because the frequencies of rotors and motors may differ. But the above mentioned method allows detecting quadcopters which produce sounds 3 decibels lower than the surrounding noises.

In the competition dedicated to the classification of sounds of birds [4] the Mel Spectrograms showed the best results. [5]

In this work for classification we applied the method used by the winners of the competition -- Mel Spec-

trograms and Resnet-50 neural network. It allowed detecting different types of quadcopters in the selected set of data.

2. MAIN NOTIONS

Mel Spectrogram is a spectrogram where frequency is expressed not in hertz, but in mel's.

There exist different ways of transform hertz to mels, and the most common is the following:

$$m = 1127 \ln\left(1 + \frac{f}{700}\right) \quad (1)$$

Mel Spectrogram helps to separate out the bass frequencies better, while they propagate in nature further than high frequencies.

The difference between a spectrogram and a Mel Spectrogram is represented in Figure 1.

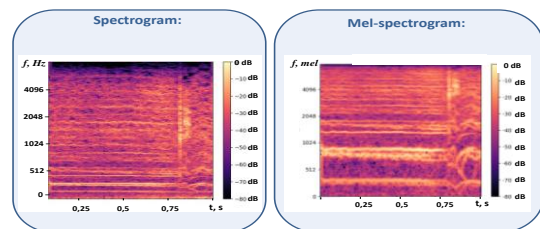


Figure 1. The difference between spectrogram and Mel Spectrogram

2.1. Description of Test dataset

In the test set of data the sounds of flying DJI P3 Pro, FPV250, DJI – Agras T30 quadcopters were used. Many different sounds occurred in the noise record, such as technical, city noise, speech, wind etc.

Each sound was saved in wav format; the soundtrack from the video from Youtube.com was also cut out and saved in wav format.

2.2. Procedure of analysis

A Mel Spectrogram of flying quadcopter is shown in Figure 2.

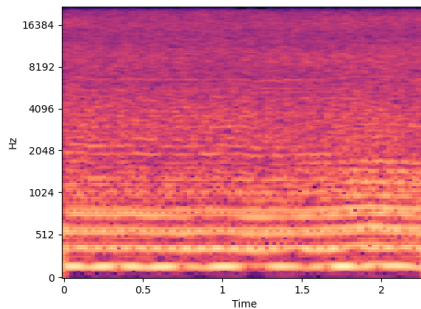


Figure 2. Mel-Spectrogram of flying quadcopter

The audio signals were read at 20000 Hz, because the equipment used to test the program for detecting quadcopter in real-time reads sounds in diapason between 20 and 20000 Hz.

Length of the windowed signal for fourier transformation for Mel-spectrogram – 1024, the amount of mels – 220, minimal frequency - 20 Hz, maximal – 20000 Hz.

The majority of quadcopters showed the activity between 0 and 1000 mels frequencies, but as we don't know, how other quadcopters will react, all frequencies, which microphone can read were displayed.

2.3. Neural Network Training

All signals (quadcopters and noise) were cut into parts by the length one second, then they were divided into training, validation and testing sets.

As a result, 1440 second-parts of flying quadcopter soundtracks, 511 validation and 1221 testing were used for training. For noise signal we used 3603 for training, 451 for validation and 1144 for testing.

For sound augmentation the following procedures were performed:

- Sound deceleration/precipitation for 5-10%
- Pitch shift for 3-5%
- Poor signal records multiplication by means of quadratic transformation
- Quadcopter sound amplification in relation

to noise and mush by power transformation with $\frac{1}{2}$ exponent

- Signal mirroring by time

The Resnet-50 neural network to detect a flying quadcopter was trained on the following data:

- Spectrograms with 2 classes: quadcopters and noises
- Spectrograms with 4 classes: quadcopter, city noises, natural noises, speech
- Mel Spectrograms with 4 classes

After that an extra training on the larger amount of data, received by link [6] was performed.

This data set is of higher quality (all these sounds were recorded with professional equipment). Each sound was classified according to quadcopter model.

For training set 8400 second-parts of quadcopter recordings were used, for validation 1994, for testing 5044. For noises 7369 in training, 1840 in validation, 27358 in testing.

This training was performed on 4 classes with Mel Spectrograms only. For the augmentation of training data set the same actions were performed.

2.4. Results of experiments

As Table 1 shows, the method of increasing of the amount of classes proved to be most effective, because we are not interested in accuracy of classes "city noises", "natural noises" and "speech" detection, if during the classification neural network doesn't relate these data to the quadcopter. The usage of Mel Spectrograms also shows significant improvement.

Table 1. The results of quadcopter detection according to classes and representations

Amount of classes	2	4	4
Training set	Sp-s	Sp-s	Mel-sp-s
Validation:			
TP, %	73.6	97.2	99.8
FP, %	25.3	3.3	0.2
Testing:			
TP, %	69.8	90.8	99.5
FP, %	29.5	9.2	0.8

The sound detection efficiency of quadcopter was higher with the larger amount of data. 1 quadcopter sound wasn't detected on validation and testing sets (~99.95% detections on validation and

~99.98% in testing) as well as 1 sound was false detected as quadcopter on validation and 2 on testing set (~0.05% and ~0.007% accordingly).

Resnet-50 neural network was trained by means of Adam optimizer with 10^{-5} learning rate.

2.5. Detection errors

The quadcopter was not detected in situations when the sound of quadcopter was in extremely noisy environment.

On the larger amount of data the amount of false positive detections decreased. Only 1 extremely noisy sound was false positively detected as quadcopter.

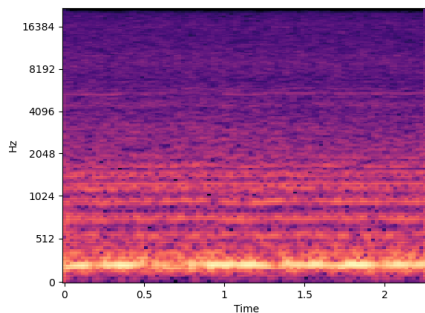


Figure 3. Quadcopter Mel-Spectrograms in noisy environment

The quadcopter was false positively detected on some natural noises (contained in class "city noises") Mel Spectrograms.

On the larger amount of data also only 2 natural noises sounds were false positively classified as quadcopter. The traffic sounds from city noises were no longer false classified as quadcopter.

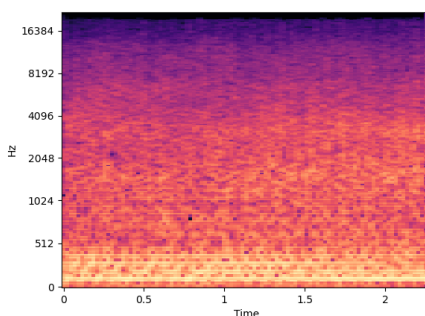


Figure 4. Natural noise Mel Spectrogram false positively detected as quadcopter

2.6. Real-time quadcopter detection software system

For real-time quadcopter detection the program was set up. It reads the sound from the microphone,

each second the signal is transformed into Mel Spectrogram and is applied to the neural network which defines the detection class. The operator receives a signal, if the quadcopter is detected or not.

The above mentioned software system is planned to be tested in real conditions.

3. CONCLUSIONS

The way of quadcopter detection implied in this work can be effectively implemented.

The use of larger amount of data increases the detection efficiency

Mel Spectrograms used for training perform the best results during the testing. The adding of different noise classes results in the significant efficiency gains as well. Moreover, the confusion of the noises does not effect on the result of detection. In further research, we are going to test the software system for real-time quadcopter detection in the field, use other signal notations for neural network training, compile the new signal samplings for neural network training and testing.

4. ACKNOWLEDGMENT

The author would like to thank Prof. N. Ampilova, St. Petersburg State University, Dept. of Mathematics and Informatics for theoretical help in digital processing area and editing this paper.

References

- [1] Samadzadegan, F.; Dadrass Javan, F.; Ashtari Mahini, F.; Gholamshahi, M. Detection and Recognition of Drones Based on a Deep Convolutional Neural Network Using Visible Imagery. *Aerospace* 2022, 9, 31. <https://doi.org/10.3390/aerospace9010031>
- [2] Baek S, Jung Y, Lee S (2021) Signal expansion method in indoor FMCW radar Systems for Improving Range Resolution[J]. *Sensors* 21(12):4226
- [3] Djurek, Ivan & Petosić, Antonio & Grubeša, Sanja & Suhanek, Mia. (2020). Analysis of a Quadcopter's Acoustic Signature in Different Flight Regimes. *IEEE Access*. 8. 1-1. 10.1109/ACCESS.2020.2965177.
- [4] <https://www.kaggle.com/c/birdsong-recognition>
- [5] S. S. Stevens and J. Volkman, E. B. Newman, "A Scale for the Measurement of the Psychological Magnitude Pitch", *The Journal of the Acoustical Society of America* 8, 185-190 (1937) <https://doi.org/10.1121/1.1915893>
- [6] <https://hissandroar.com/v3/soundlibrary/sd024-quadcopter-uav-drone>

HAND INFLUENCE ON THE MOBILE PHONE ANTENNAS' MATCHING TO THE FREE SPACE

Tamar Nozadze², Mtvarisa Kurtsikidze¹, Veriko Jeladze², Giorgi Ghvedashvili²

1- Samtskhe-Javakheti State University

2- Ivane Javakhishvili Tbilisi State University, Laboratory of Applied Electrodynamics and Radio Engineering

3, Chavchavadze Ave. 0176, Tbilisi, Georgia

E-mail: tamar.nozadze@tsu.ge, E-mail: mtvarisakurtsikidze@gmail.com,

E-mail: veriko.jeladze@tsu.ge, E-mail: giorgi.ghvedashvili@tsu.ge,

Abstract

The goal of the research is to study the thermal effects caused by the electromagnetic (EM) field emitted by the mobile phone antenna. A novelty of the study is the Hand Influence consideration on the Mobile Phone Antennas' matching to the free space.

Inhomogeneous human model with different positions of the hand (fingers) and at different distances (1 mm, 10 mm, 20 mm) from the human head to the headset are studied;

The mobile phone antenna matching study to free space was carried out using the Finite-Difference Time-Domain (FDTD) method.

3700 [MHz] standard communication frequency was selected for numerical simulations.

1. INTRODUCTION

Mobile phones have recently become an integral part of our lives. Naturally, interest arose in their impact on human health. Electromagnetic fields (EMF) emitted from mobile phone antennas interact with the human head and other parts of the body, which in some cases can affect human health. Exposure to these electromagnetic fields is inversely proportional to the distance between the head and the mobile phone. But during communication, in most cases, the mobile phone antenna is in close proximity to the sensitive tissues of the human head. Therefore, the study of possible side effects associated with it is very relevant and important today.

As it is known, the energy absorption of EMF in tissues is characterized by the SAR coefficient (specific absorption coefficient [W / kg]), which is determined by the power absorbed by the unit of mass of the tissue. SAR is the only safety criterion for assessing the effects of this radiation on humans. Its thresholds are set by the Federal Communications Commission (FCC) in the USA and the International Commission on Non-Ionizing Radiation Protection (ICNIRP) in Europe [1]. Existing studies have shown that the interaction between an EM field and a biological object depends on the characteristics of the emitter [2]: its frequency, its location, and its orientation toward the object; On

the shape of the emitted wave and the amplitude value of the EM field; As well as the ability of the biological body to absorb and accumulate energy [3].

Many publications show that absorption of radiated energy (SAR) depends on mobile phones and antenna types [4-5], its positions, and radiated power from the mobile phones [6]. The radiation nature and EM fields behaviour depends on complex human body geometry [8], user's hand positions, other objects' existence around the user; where the user is located, in an enclosed or semi-enclosed space. But it's impossible to thoroughly quantitatively consider all these details.

Modern smartphones have AGC (Automatic Gain Control) and automatically increase the radiation power to establish a good connection in case the signal from the base station is weakened. The reactive field around the antenna increases. Because the reactive field area is larger than a cell phone with a hand, it covers all nearby objects with the ear, head, and hand. The result will be a large absorption at high reactive fields, which can be dangerous for humans' health [9].

The negative effects associated with these impacts are cumulative nature and may appear in the future. Of particular note are the harmful effects on children. They are exposed to RF radiation from an early age. The brain is the "main target organ" for

this EM radiation. The nervous system of children and the brain are still unformed, the tissue composition is relatively different (contains a relatively large amount of water, which has a permeability, the children's skull is much thinner, more permeable to this radiation than adults and therefore the negative impact in children can be more serious [8].

The goal of the proposed research is to investigate: how the hand and fingers different positions affects on the phone radiation parameter (S11 coefficient), which describes antenna matching to the free space.

2. METHODOLOGY

Since, the real experiments on human is not permitted, we will investigate scheduled tasks, by means of computer modelling. The Finite-Difference Time-Domain (FDTD) method [6], [9] will be used for numerical simulations. FDTD is the most suitable numerical method for computational analysis of complex-shaped and inhomogeneous objects like the human body. It gives us ability to use realistic nonhomogeneous human model in our research. However, the disadvantage of FDTD method is that we can't estimate the calculation error. Numerical experiments will be carried out using the EM and thermal solver of the proprietary FDTD based program package "FDTDLab", developed at TSU (Laboratory of Applied Electrodynamics of the Tbilisi State University). The woman computer head model, named "Ella", a 3D model with 1 mm discretization from "Virtual Population" (IT²S Foundation) will be used for EM exposure simulations. Different hand configurations in holding the mobile phone (with different types of antennas) will be created by us (for example, phone held by fingers and phone held and covered by the palm) [9]. The considered head model consists of 47 types of tissues with different dielectric properties. For simplicity, the hand model will be filled with muscle material.

Frequency-dependent tissue parameters will be used from the known database (<https://itis.swiss/virtualpopulation/tissueproperties/database/database-summary/>) A sinusoidal waveform of 3700 MHz frequency will be used for simulations.

For the human head model, two hand positions were prepared: When the mobile phone is held with fingers tip (**hand 1**), and when the mobile phone is held tightly with hand, touches the hand palm (**hand 2**), **Figure 1**.

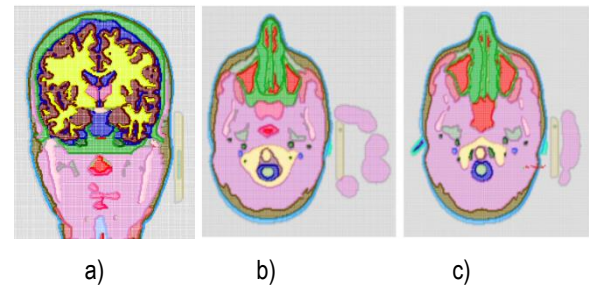


Figure 1. Woman discrete model: (a) without hand, (b) with hand position 1, (c) with hand position 2. at 3700 MHz

The mobile phone dimensions were (L × W × H) 5 × 0.8 × 9 [cm], with the dipole antenna embedded. The phone case permittivity was $\epsilon = 2$.

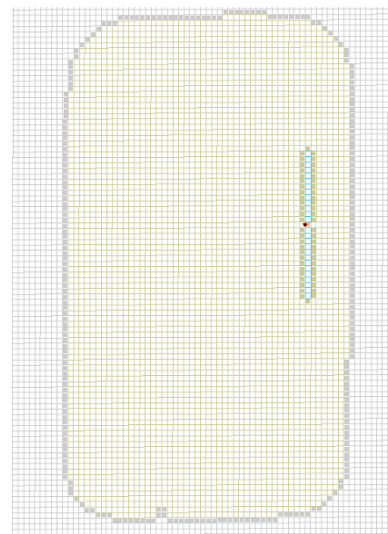


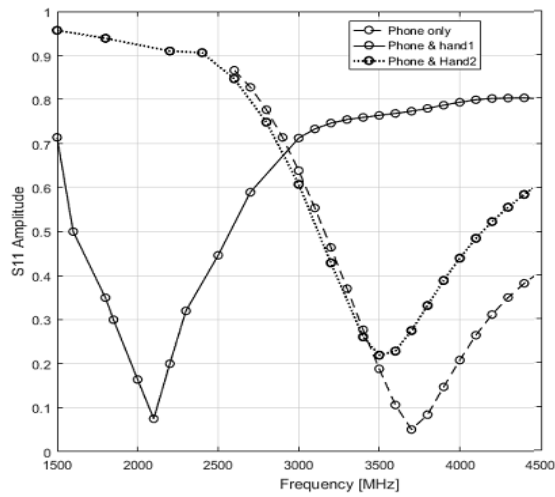
Figure 2. Mobile phone model with Dipole antenna.

The dipole length for the selected frequencies (3700 MHz) was selected so the S11 coefficient to be the lowest possible. In this case, the best antenna matching to open space was obtained. The length of the dipole antenna was 0.26 mm while the minimal S11 was 0.08 **Figure 2**.

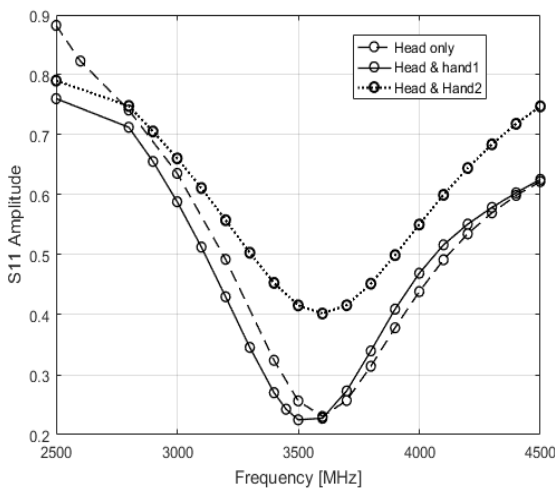
3. RESULTS OF NUMERICAL SIMULATIONS AND DISCUSSIONS

We studied frequency characteristics for a considered dipole antenna at the considered frequency, as it is shown in **Figure 3**.

In both cases of numerical experiments hand considerations increase the S11 coefficient. In some cases, the head, hand, or fingers different positions reduce the S11 coefficient (this means that the antenna is well matched but at the shifted frequencies).



a)



b)

Figure 3. Dipole antenna frequency characteristics: a) head without hand, b) head with hand 1, and hand 2.

When mobile phone antenna is hold with a hand figures (hand 1) bad matching is observed (with and without head consideration) compared to the case when the mobile phone is covered with a hand palm (hand 2) **Figure 3**.

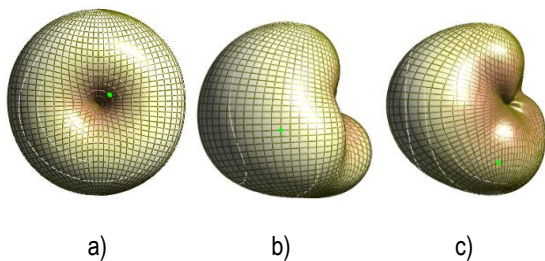


Figure 4. 3D radiation patterns for the mobile antenna without a head model at 3700 MHz: a) only phone, b) phone+hand 1, c) phone+hand 2.

The 3D radiation patterns for the mobile antenna without a head and with different hand configurations are shown in **Figure 4, 5**. It is well seen that

the radiation patterns for the fixed-gain depended on the modeling scenarios.

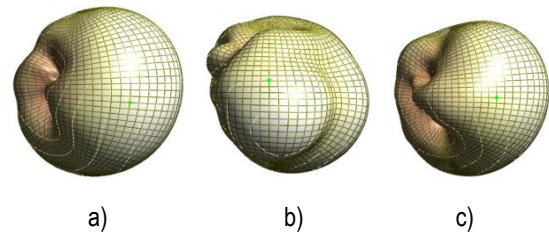


Figure 5. 3D radiation patterns for the mobile antenna with a head model at 3700 MHz: a) phone+only head, b) phone+head and hand 1, c) phone+head and hand 2

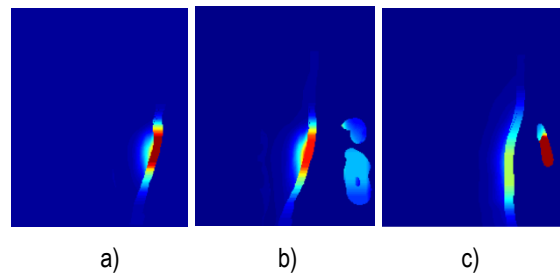


Figure 6. SAR distribution inside the human head-hand models at 3700 MHz: a) head without a hand, b) head and hand 1, c) head and hand 2

Point SAR distribution inside the head-hand models is illustrated in **Figure 6**. When the hand is considered, peak SAR locations were observed inside the hand. Because hand absorbs a big part of the EMF energy and therefore, SAR peak values in the head tissues are reduced.

4. CONCLUSION

In the present study, we investigated the impact of hand and head on mobile phone antenna matching conditions. The obtained results showed that hand consideration changes the antenna matching to the free space significantly.

The results of the research will be of great importance to each of us, and it will have a potential impact on the relevant industry and the wider community.

Research is not completed. The problems raised in the proposed paper are most significant and need further researches.

5. ACKNOWLEDGMENTS

The study is financially supported by Joint Rustaveli-DAAD-fellowship programme, 2022, (N # 04/12).

References

- [1] ICNIRP, "Guidelines for limiting exposure to timevarying electric, magnetic and electromagnetic fields (up to 300 GHz)," *Health Physics*, vol. 74, pp. 494-522, April 1998.
- [2] J. Krogerus et al., "Effect of the human body on total radiated power and the 3-d radiation pattern of mobile handsets," *IEEE Trans. Instrum. Meas.*, 56(6), p. 2375–2385, 2007.
- [3] M. R. I. Faruque, et al., "Effect of human head shapes for mobile phone exposure on electromagnetic absorption," *Informacije MIDEM-Journal of Microelectronics, Electronic Components and Materials*, 40(3), pp. 232-237, 2010.
- [4] M. R. I. Faruque et al., "Effects of Mobile Phone Radiation onto Human Head with Variation of Holding Cheek and Tilt Positions," *Journal of Applied Research and Technology*, vol. 12, pp. 871-876, October 2014.
- [5] N. B. Rahman, et al., (2017) AzemiImpedance Analysis of Mobile Phone Antenna in the Presence of User's Hand. 2017 International Conference on Emerging Electronic Solutions for IoT (ICEESI 2017). <https://doi.org/10.1051/mateconf/201714001031>
- [6] T. Nozadze, V. Jeladze, R. Zaridze, 'Mobile Antenna Matching Study Considering Different Holding Positions at 2100 MHz Frequency', XXVIth International Seminar/Workshop on Direct and Inverse Problems of Electromagnetic and Acoustic Wave Theory DIPED-2021, Tbilisi, Georgia, September 15-18, 2020
- [7] V. Jeladze, M. Tsverava, T. Nozadze, V. Tabatadze, M. Prishvin and R. Zaridze, "EM exposure study on inhomogeneous human model considering different hand positions," XXI-th International Seminar/Workshop on Direct and Inverse Problems of Electromagnetic and Acoustic Wave Theory (DIPED 2016), Tbilisi, Georgia, September 26-29, 2016, pp. 9-12.
- [8] J. Keshvari, M. Kivento, A. Christ and G Bit-Babik. "Large scale study on the variation of RF energy absorption in the head & brain regions of adults and children and evaluation of the SAM phantom conservativeness", *Phys. Med. Biol.* 61 (2016) 2991–3008.
- [9] V. Jeladze, T. Nozadze, I. Petoev-Darsavelidze & B. Partsvania, "Mobile phone antenna-matching study with different finger positions on an inhomogeneous human model", *Electromagnetic Biology and Medicine*, Volume 38, 2019 - Issue 4. Published Online: 14 Jul 2019. <https://doi.org/10.1080/15368378.2019.1641721>

FPGA BASED EDGE DETECTION: INTEGER SQUARE ROOT ALGORITHM

Dimitre Kromichev

Department of Marketing and International Economic Relations, University of Plovdiv
24 Tzar Asen Str, Plovdiv 4000, Bulgaria

dkromichev@yahoo.com

Abstract

In FPGA based edge detection which uses gradients to find contours, the calculation of integer square root focused on both accuracy and speed presents a serious problem. In this paper, proposed is an integer square root algorithm. Its application is focused on computing the gradient magnitude in FPGA based edge detection. The algorithm is explored for mathematical accuracy, maximum operating frequency and minimum number of clock cycles on the basis of ten Intel (Altera) FPGA families. It is ascertained that the algorithm guarantees total mathematical accuracy. Its maximum operating frequency is higher than the maximum operating frequency of embedded memory, and it requires a single clock cycle to execute. The proposed algorithm's capabilities are assessed on a comparative basis.

1. INTRODUCTION

In FPGA based edge detection which relies on gradient to detect image contours the accuracy of the obtained gradient magnitude value depends on the accuracy of square root calculations. Hardware implementation of integer square root is a serious problem due to the complexity of computations. Hence the most widely used approach is to prioritize speed over mathematical accuracy by resorting to different approximation patterns. The latter generally have a strong negative impact on the quality of detected contours. Therefore, when the focus is on both achieving the ultimate execution speed and guaranteeing the detected contours' quality FPGA based edge detection using gradient requires an integer square root algorithm which is capable of: 1) providing mathematically accurate result for the smallest possible count of clock cycles; 2) working at a clock frequency which is higher than the maximum operating frequency of the component defining the upper limit of clock frequency in FPGA based edge detection.

The algorithm which most current FPGAs use is radix 2 digit recurrence square root [5][6]. Digit recurrence methods rely on subtractions and iterations [8]. Hence, they have limited performance in hardware [7][15]. Another approach is the functional iteration which is divided into additive and multiplicative according to the operation used in each iterative step [3][9]. Newton-Raphson method has the disadvantage of using division [1]. FPGA focused

modifications include: modified nonrestoring square root using only subtraction [12][13][14]; nonrestoring pipelined square root using only subtraction [4]; square root based on linear approximation subsystem with Look-up tables [10][11]; square root based on subtractors and multipliers - appropriate only for small numbers [16]; square root based on successive subtraction of odd integers [2].

The objective of this paper is to propose an integer square root algorithm. Its application is focused on computing the gradient magnitude in FPGA based edge detection. The task is to explore the algorithm for mathematical accuracy, maximum operating frequency and minimum number of clock cycles in ten Intel (Altera) FPGA families. Used tools: Scilab, Intel (Altera) Quartus, TimeQuest Timing Analyzer, ModelSim. The hardware description language is VHDL. Relevant to the conducted analyses and drawn conclusions are gray scale images.

2. THE PROPOSED INTEGER SQUARE ROOT ALGORITHM

The difference between the squares of any two integers is presented by

$$\begin{aligned}n^2 - (n-p)^2 &= 2(n-p)p + p^2 & (1) \\ p \in \mathbb{N}, p \geq 1, p < n, \\ n \in \mathbb{N}.\end{aligned}$$

For $p=1$ (1) becomes

$$n^2 - (n-1)^2 = 2(n-1) + 1. \quad (2)$$

From (2) it follows that:

- The difference Dsq between the squares of any two consecutive integers $n-1$ and n is a constant represented by an odd number

$$Dsq = 2(n-1) + 1. \quad (3)$$

- The difference between any two consecutive differences is a constant

$$Dsq - (Dsq - 1) = 2. \quad (4)$$

Hence, the following sequence can be defined

$$(((n+2)^2 - (n+1)^2) - ((n+1)^2 - n^2))_{n=0}^{\infty} \quad (5)$$

Thus, every single number $r \in N$ represents a radical which pertains to a specific interval $[n^2 - (n-1), n^2 + n]$ by satisfying the inequalities

$$r \geq n^2 - (n-1) \ \& \ r \leq n^2 + n. \quad (6)$$

All radicals included in $[n^2 - (n-1), n^2 + n]$ are associated with a single integer n which represents the square root result according to

$$n = \sqrt{[n^2 - (n-1), n^2 + n]}. \quad (7)$$

The accuracy of integer square root result depends on rounding. On the basis of (3), (4) and (5), the left- and rightmost values of $[n^2 - (n-1), n^2 + n]$ include rounding and guarantee mathematical accuracy.

3. COMPUTATIONAL MECHANISM IN FPGA

Application of the algorithm: gradient magnitude computation in FPGA based edge detection.

The upper limit of clock frequency of FPGA based edge detection which relies on gradient is defined by the maximum operating frequency of embedded memory. The smallest possible count of clock cycles required by an integer arithmetic operation to execute is 1. Therefore, the goal of the algorithm is: guarantee that for all possible values of the radical in edge detection

$$\begin{aligned} F_{\max}(squareIn) &> F_{\max}(embMem) \\ nTclk_{\min}(squareIn) &= const = 1 \end{aligned} \quad (8)$$

where

$F_{\max}(embMem)$ is the maximum operating frequency of embedded memory,

$F_{\max}(squareIn)$ is the maximum operating frequency of the proposed algorithm,

$nTclk_{\min}(squareIn)$ is minimum number of clock cycles required by the proposed algorithm to execute.

In edge detection, all radicals are within $[0, (2^8-1)^2 + (2^8-1)^2]$. In FPGA, the computational mechanism includes four steps:

Step #1. The value of gradient magnitude is within $[0, 2^8-1]$. Because $\sqrt{0}=0$, $r=0$ is a special case and a separate interval is not used. Thus, radicals are distributed across 2^8-1 intervals according to (3), (4), (5), (6) and (7).

Step #2. Each of these intervals is associated with a single integer within $[1, 2^8-1]$.

Step #3. The boundaries of all intervals are checked simultaneously. Of all checks, only for a single interval the boolean result is true. Thus the square root calculation is checking if a radical fits within the boundaries of a particular interval.

Step #4. The integer associated with this interval is the accurate integer square root result.

The model of computational mechanism is presented in Figure 1.

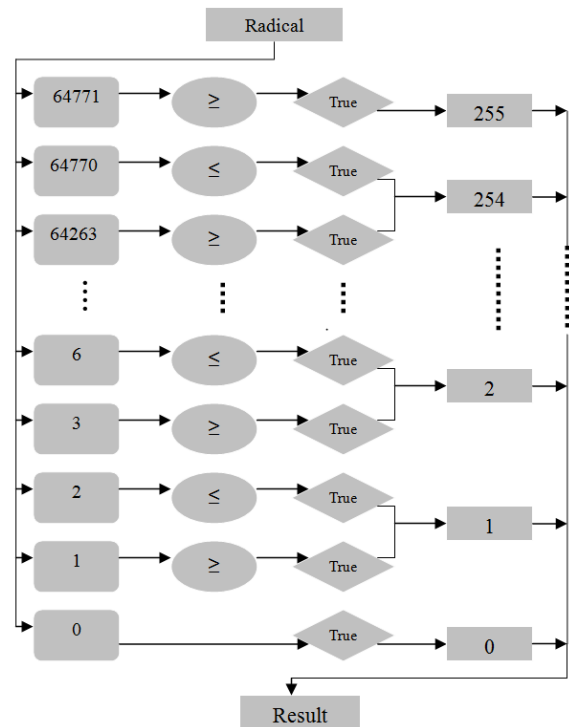


Figure 1. The model of computational mechanism of the algorithm

The RTL design is in Fig. 2.

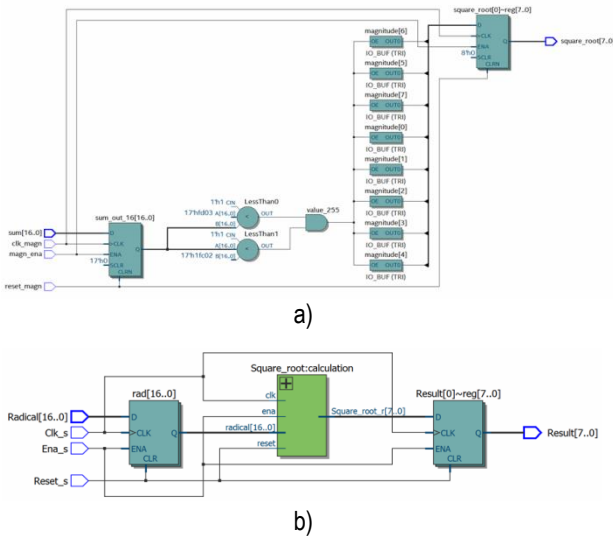


Figure 2. RTL design of a single interval calculation (a) and the entire algorithm (b) (Source: Intel (Altera) Quartus)

Resource utilization is in Table 1.

Table 1. Resource utilization of the proposed algorithm

FPGA family	Utilization by different resource types				
	Logic utilization (in LEs/ALUTs/ALMs)	Total registers	Total memory bits	Total DSP blocks	Embedded multiplier 9 bit elements
Cyclone	1461 (LEs)	-	0	-	0
Cyclone II	1386 (LEs)	272	0	-	0
Cyclone III	1290 (LEs)	264	0	-	0
Cyclone IV	1290 (LEs)	264	0	-	0
Cyclone V	487 (ALMs)	264	0	0	-
Stratix	1249 (LEs)	288	0	0	-
Stratix II	1014 (ALUTs)	282	0	0	-
Stratix III	992 (ALUTs)	270	0	0	-
Stratix IV	992 (ALUTs)	279	0	0	-
Stratix V	483 (ALMs)	270	0	0	-

4. PROVING THE ALGORITHM'S MATHEMATICAL ACCURACY

The proposed algorithm is tested for mathematical accuracy using all possible values of the radical in FPGA based gradient magnitude.

Critical to the mathematical accuracy of an integer square root algorithm is the accurate rounding. Sample results are presented below.

Check # 1

Radical: 35984. Therefore the interval is [35911, 36290]. The reference value is 190. This is the result. Conventional square root result: **189.6944912220700203.**

Check # 2

Radical: 33800. Therefore the interval is [33673, 34410]. The reference value is 184. This is the result. Conventional square root result: **183.8477631085023563.**

Check # 3

Radical: 42353. Therefore the interval is [42231, 42642]. The reference value is 206. This is the result. Conventional square root result: **205.7984450864486002.**

Check # 4

Radical: 37370. Therefore the interval is [37057, 37442]. The reference value is 193. This is the result. Conventional square root result: **193.3132173442881789.**

Another approach to proving accuracy is checking the boundary values of the intervals. Ten sample checks are presented in Table 2.

Table 2. Proving the accuracy by checking the boundary values of the intervals

Intervals under test	Conventional square root result (before rounding)		Result calculated with integer square root algorithm based on intervals
	Result of square root for the interval's leftmost value before rounding	Result of square root for the interval's rightmost value before rounding	
[63253, 63756]	251.501491	252.499504	252
[46441, 46872]	215.501740	216.499422	216
[43057, 43472]	207.501807	208.499400	208
[32221, 32580]	179.502089	180.499307	180
[26083, 26406]	161.502321	162.499230	162
[10921, 11130]	104.503588	105.498815	105
[7657, 7832]	87.504285	88.498587	88
[4161, 4290]	64.505813	65.498091	65
[343, 380]	18.520259	19.493588	19
[91, 110]	9.539392	10.488088	10

These checks prove that the proposed algorithm guarantees total mathematical accuracy.

5. EXPLORING $F_{max}(squareInt)$ AND $nTclk_{min}(squareInt)$ IN FPGA

Exploration methodology:

- The algorithm is implemented using all values in $[0, (2^8-1)^2 + (2^8-1)^2]$.

The results are shown in Table 3.

Table 3. $F_{max}(squareInt)$ and $nTclk_{min}(squareInt)$ of the proposed algorithm

FPGA family	$F_{max}(squareInt)$ (in MHz)	$nTclk_{min}(squareInt)$
Cyclone	195	1
Cyclone II	286	1
Cyclone III	320	1
Cyclone IV	322	1
Cyclone V	329	1
Stratix	289	1
Stratix II	414	1
Stratix III	538	1
Stratix IV	586	1
Stratix V	613	1

Test results prove the functional capabilities of the proposed integer square root algorithm:

- Total mathematical accuracy of results

- $F_{\text{mK}}(\text{squareIn}) > F_{\text{mK}}(\text{embMem})$ for all values of radical which can be calculated in FPGA based gradient edge detection
- $n\text{Tclk}_{\text{min}}(\text{squareIn}) = \text{const} = 1$.

All existing integer square root algorithms have two stages:

Stage #1. Execute operation square root over a radical r

$$\sqrt{r} = n^* \quad (9)$$

where

n^* is the square root result before rounding.

Stage #2. Execute rounding to obtain mathematical accurate square root result n

$$n^* + 0/1 = n \quad (10)$$

In the proposed integer square root algorithm based on intervals, Stage #1 and Stage #2 are combined into a single operation executed as a number of parallel comparisons. Therefore, with respect to the technology of executing comparison in FPGA, $F_{\text{mK}}(\text{squareIn})$ depends on the propagation delay of ripple carry adder and sign check operation.

The proposed algorithm's speed characteristics are assessed on a comparative basis using the radix-2 iterative square root algorithm. The comparison between $F_{\text{mK}}(\text{squareIn})$ and the highest operating frequency of the radix-2 iterative square root $F_{\text{mK}}(\text{IterativeSquare})$ is conducted on the basis of executing the iterative square root within two clock cycles – a separate clock cycle is used for rounding. The comparison results show that $F_{\text{mK}}(\text{squareIn})$ is higher than $F_{\text{mK}}(\text{IterativeSquare})$ from 82.9% to 87.1%.

6. CONCLUSION

Proposed is an integer square root algorithm. Its application is focused on calculating gradient magnitude in FPGA based edge detection. The algorithm is explored for mathematical accuracy, maximum operating frequency and minimum number of clock cycles in ten Intel (Altera) FPGA families. Exploration results are assessed on a comparative basis using radix-2 iterative square root.

References

- [1] Addanki Purna Ramesh and I. Jayaram Kumar, "Implementation of Integer Square Root," International Journal of Engineering Science and Innovative Technology (IJESIT), Volume 4, Issue 1, January 2015, pp. 105-113
- [2] Aiman Zakwan Jidin and Tole Sutikno, "FPGA Implementation of Low-Area Square Root Calculator," TELKOMNIKA, Vol. 13, No. 4, December 2015, pp. 1145~1152
- [3] Anuja Nanhe, Gaurav Gawali, Shashank Ahire, and K. Sivasankaran, "Implementation of Fixed and Floating Point Square Root Using Nonrestoring Algorithm on FPGA," International Journal of Computer and Electrical Engineering, vol. 5, no. 5, 2013, pp. 533-537
- [4] Arpita Jena and Siba Ku Panda, "FPGA-VHDL Implementation of Pipelined Square root Circuit for VLSI Signal Processing Applications," International Journal of Computer Applications, Volume 142 – No.5, May 2016
- [5] Fernando Martin del Campo, Alicia Morales-Reyes, Roberto Perez-Andrade, Rene Cumplido and Aldo G. Orozco-Lugo Claudia Feregrino, "A multi-cycle fixed point square Root and module for FPGAs," IEICE Electronics Express, Vol. 1 – No. 7, 2008, pp. 957-966
- [6] Florent de Dinechin, Mioara Maria Joldes, Bogdan Pasca, and Guillaume Revy, "Multiplicative square root algorithms for FPGAs.," International Conference on Field Programmable Logic and Applications, Aug 2010, pp.14-17
- [7] G. Anupama and A. Raghuram, "Novel Square Root Algorithm and its FPGA Implementation," International Journal of Engineering and Technical Research (IJETR), Vol. 3 (10), 2015, pp. 64-67
- [8] Muhazam Mustapha, Burinieamman Jayabalan and Anis Shahida Niza Mokhtar, "Intel/Altera FPGA Implementation of CORDIC Square Root Algorithm," Journal of Computer Science & Computational Mathematics, Vol. 11, Issue 3, September 2021, pp. 52-56
- [9] Palchadhuri and Rajat Subhra Chakraborty, "High Performance Integer Arithmetic Circuit Design on FPGA: Architecture, Implementation and Design Automation," Springer, 2016
- [10] Purna Ramesh Addanki, "Implementation of Integer Square Root," International Journal of Engineering Science and Innovative Technology (IJESIT), Vol. 4 (1), 2015, pp. 104-112
- [11] S. Lachowicz and H-J. Pfeleiderer, "Fast Evaluation of the Square Root and Other Nonlinear Functions in FPGA," IEEE International Symposium on Electronic Design, Test & Applications - DELTA, 2008, pp. 474-477
- [12] Tole Sutikno, "An Optimized Square Root Algorithm for Implementation in FPGA Hardware," TELKOMNIKA, Vol. 8, No. 1, 2010, pp. 1 – 8
- [13] Tole Sutikno, "An Efficient Implementation of the Non Restoring Square Root Algorithm in Gate Level," Inter-

- national Journal of Computer Theory and Engineering, Vol.3, (1), 2012, pp. 46-51
- [14] Tole Sutikno, Aiman Zakwan Jidin, Auzani Jidin and Nik Rumzi Nik Idris, "VHDL Coding of Modified Non-Restoring Square Root Calculator," International Journal of Reconfigurable and Embedded Systems (IJRES) , Vol. 1 (1), 2012, pp. 37~42
- [15] Vladitiu, M., Computer Arithmetic: Algorithms and Hardware Implementations, 2012
- [16] Zhongcheng Zhou and Jingchun Hu, "A Novel Square Root Algorithm and its FPGA Simulation," Journal of Physics: Conference Series, Volume 1314, 3rd International Conference on Electrical, Mechanical and Computer Engineering 9–11 August 2019, pp. 168-176

FPGA BASED EDGE DETECTION: INTEGER INVERSE TANGENT ALGORITHM

Dimitre Kromichev

Department of Marketing and International Economic Relations, University of Plovdiv
24 Tzar Asen Str, Plovdiv 4000, Bulgaria

dkromichev@yahoo.com

Abstract

FPGA based edge detection targeting ultimate execution speed and relying on gradient direction to define image contours has to tackle the problem of computing integer inverse tangent both accurately and fast. This paper presents an integer inverse tangent algorithm. It is designed to be used in the gradient direction submodule of FPGA based edge detection computations. Having investigated the mathematical accuracy, maximum operating frequency and minimum number of clock cycles on the basis of ten Intel (Altera) FPGA families, it is ascertained that the proposed algorithm is capable of securing total accuracy and working at a frequency higher than the maximum operating frequency of embedded memory under all test conditions. It takes only three clock cycles to provide an accurate result.

1. INTRODUCTION

Because the hardware implementation of integer inverse tangent is complicated and slow, approximation patterns are employed as a tool of choice. In edge detection which uses gradient direction, detected contours' quality is negatively impacted by the inaccuracy of inverse tangent. Therefore, in FPGA based edge detection focused on ultimate execution speed, it is a must that the inverse tangent can guarantee total mathematical accuracy. The latter must be achieved within the same number of clock cycles required by the gradient magnitude submodule to execute, taking into account that gradient magnitude and gradient direction submodules work in parallel in FPGA.

In [3] FPGA based design targets the speeding up of \tan^{-1} computations. The results are: execution time is 320 ns; accuracy is $<0.01^\circ$. Taylor series expansion method is applied to transfer \tan^{-1} to a polynomial form [3][11]. In [6] two-argument \tan^{-1} is implemented in FPGA by using the piecewise polynomial approximation method with non-uniform segmentation. The inputs (x and y) are divided using radix-2 non-restoring division and the result is used as an input to Atan . The results are: maximum error ratio - 2.62%; execution time in Xilinx Spartan 6 - 260.5 ns. In FPGA based design of two-argument \tan^{-1} [9][8][10] division of the two inputs is implemented by a logarithmic transformation using subtraction. In [2] studied is the FPGA implementation of fixed-point two-argument \tan^{-1} by

comparing CORDIC with two multiplier based techniques. It is concluded that CORDIC is faster than the multiplier and table-based methods. In [12] presented are several approximations for four quadrant \tan^{-1} using Lagrange interpolation and optimization techniques. It is concluded that second-order polynomial provides a favorable compromise between accuracy and computational cost and is well suited for implementation in hardware. In [5] it is pointed out that long latency is a main disadvantage of methods based on CORDIC, conventional LUTs and polynomial approximation. In [1] proposed is atan2 using look-up table with 101-points. The accuracy is increased by linear interpolation. The achieved frequency is 60 MHz. The conclusion is: the accuracy of the proposed method is better than the approximation techniques. In [4] proposed is a high-accuracy computation of fixed-point \tan^{-1} using CORDIC and fast magnitude estimation. Maximum phase error is reduced from 414 LSB (angle error of 0.6355 rad) to 4 LSB (angle error of 0.0061 rad). In [7] described is an FPGA implementation of \tan^{-1} which is based on using CORDIC using serial and pipelined CORDIC architectures.

The objective of this paper is to propose an integer inverse tangent algorithm targeting the computation of gradient direction in FPGA based edge detection. The mathematical accuracy, maximum operating frequency and minimum number of clock cycles of the algorithm must be investigated using ten Intel (Altera) FPGA families. The employed tools are: Scilab, Intel (Altera) Quartus, VHDL, TimeQuest

Timing Analyzer, ModelSim, The analyses and conclusions are relevant to gray scale images.

2. THE PROPOSED INTEGER INVERSE TANGENT ALGORITHM

Application of the algorithm: computation of gradient direction. Goal of the algorithm: guarantee that

$$F_{\max}(\tan^{-1} Int) > F_{\max}(embMem)$$

$$nTclk_{\min}(\tan^{-1} Int) = const = 3 \quad (1)$$

where

- $F_{\max}(embMem)$ is maximum operating frequency of embedded memory,
- $F_{\max}(\tan^{-1} Int)$ is maximum operating frequency of the proposed algorithm,
- $nTclk_{\min}(\tan^{-1} Int)$ is minimum number of clock cycles required by the algorithm to execute.

Because the gradient direction values can only be 0, 90, 45 and 135, four equations are defined:

$$\tan^{-1}\left(\frac{G_y}{G_x}\right) = 0 \quad (2)$$

where

G_y is y gradient, $G_y \in [-255, 255]$

G_x is x gradient, $G_x \in [-255, 255]$,

$$\tan^{-1}\left(\frac{G_y}{G_x}\right) = 45 \quad (3)$$

$$\tan^{-1}\left(\frac{G_y}{G_x}\right) = 90 \quad (4)$$

$$\tan^{-1}\left(\frac{G_y}{G_x}\right) = 135 \quad (5)$$

Solving (2), (3), (4) and (5) requires finding the domains of four functions with predefined ranges

$$A_0 = \tan^{-1}\left(\frac{m_0}{n_0}\right) \quad (6)$$

$$A_{45} = \tan^{-1}\left(\frac{m_{45}}{n_{45}}\right) \quad (7)$$

$$A_{90} = \tan^{-1}\left(\frac{m_{90}}{n_{90}}\right) \quad (8)$$

$$A_{135} = \tan^{-1}\left(\frac{m_{135}}{n_{135}}\right) \quad (9)$$

where

$A_0, A_{45}, A_{90}, A_{135}$ are angular sectors in which the axes 0, 45, 90 and 135 are bisectors,

$m_0, n_0, m_{45}, n_{45},$

$m_{90}, n_{90}, m_{135}, n_{135}$ are independent variables and $m_0,$

$n_0, m_{45}, n_{45}, m_{90},$

n_{90}, m_{135}, n_{135} are within $[-255, 255]$.

Therefore, the task is to define the complete set of values for the independent variables in (6), (7), (8) and (9). To accomplish this task, the following aspects must be considered:

1) In order to avoid division by 0 the operation division must not be used.

2) The axes for 0, 45, 90 and 135 are further divided into two pairs. The ingredients of each pair are orthogonal. Hence, the angular sectors for 45 and 135 are symmetrical with respect to the x-axis. Therefore

$$|m_{45}| = |m_{135}| \quad (10)$$

and

$$|n_{45}| = |n_{135}| \quad (11)$$

As a result, the difference between 45 and 135 is based on sign relations.

3) Unlike 45 and 135, the difference between 0 and 90 is defined by the fact that their angular sectors are symmetrical with respect to axis 45. As a result, the difference between 0 and 90 is based on comparison with respect to the boundaries of the angular sector for 45.

3. COMPUTATIONAL MECHANISM IN FPGA

The algorithm includes:

Step #1. Determine all combinations between the signs of G_y and G_x .

Step #2. Define two reference points: 22.5° and 67.5° .

Step #3. Determine a numerical equivalent to angle 22.5° . The accurate representation of angle 22.5° is the fraction $\frac{99}{239}$:

$$\tan^{-1}\left(\frac{99}{239}\right) = 22.500605394851^\circ$$

Step #4. Determine a numerical equivalent to angle 67.5° . The accurate representation of angle 67.5° is the fraction $\frac{169}{70}$:

$$\tan^{-1}\left(\frac{169}{70}\right) = 67.500605394851^\circ.$$

Step #5. Calculate gradient direction Dir by simultaneously executing expressions:

If $(G_y > 0 \& G_x > 0)$ or $(G_y < 0 \& G_x < 0)$ then

If $|G_x| * 99 \geq |G_y| * 239$

$Dir = 0$

If $|G_x| * 99 < |G_y| * 239 \& |G_x| * 169 > |G_y| * 70$

$Dir = 45$

If $|G_x| * 169 \leq |G_y| * 70$ $Dir = 90$

If $(G_y > 0 \& G_x < 0)$ or $(G_y < 0 \& G_x > 0)$ then

If $|G_x| * 99 \geq |G_y| * 239$ $Dir = 0$

If $|G_x| * 99 < |G_y| * 239 \& |G_x| * 169 > |G_y| * 70$

$Dir = 135$

If $|G_x| * 169 \leq |G_y| * 70$ $Dir = 90$

If $G_y = 0 \& G_x \neq 0$ $Dir = 0$

If $G_y \neq 0 \& G_x = 0$ $Dir = 0$

If $G_y = 0 \& G_x = 0$ $Dir = 0$. (12)

The computational mechanism in FPGA is presented in Figure 1.

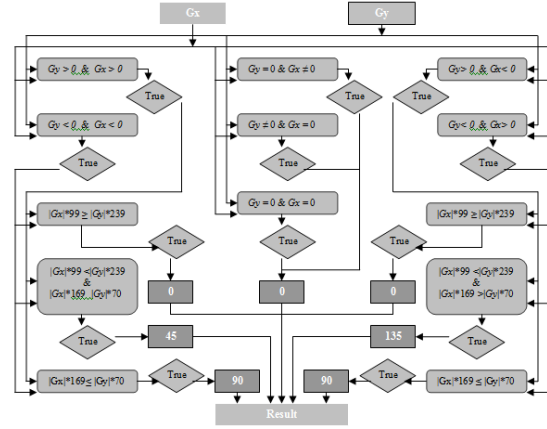


Figure 1. The model of computational mechanism in FPGA

The RTL design of the algorithm is shown in Figure 2.

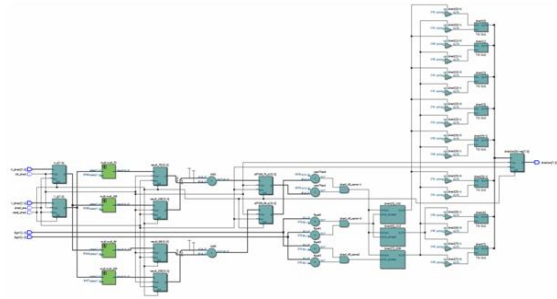


Figure 2. RTL design of the algorithm (Source: Intel (Altera) Quartus)

Resource utilization is presented in Table 1.

Table 1. Resource utilization of the proposed algorithm

FPGA family	Utilization by different resource types				
	Logic utilization	Total registers	Total memory bits	Total DSP blocks	Embedded multiplier 9 bit elements
Cyclone	118 (LEs)	-	-	-	-
Cyclone II	94 (LEs)	74	-	-	4
Cyclone III	80 (LEs)	38	-	-	4
Cyclone IV	80 (LEs)	38	-	-	4
Cyclone V	30 (ALMs)	38	-	4	-
Stratix	104 (LEs)	64	-	3	-
Stratix II	80 (ALUTs)	50	-	3	-
Stratix III	65 (ALUTs)	40	-	3	-
Stratix IV	65 (ALUTs)	40	-	3	-
Stratix V	32 (ALMs)	40	-	2	-

4. PROVING THE ALGORITHM'S MATHEMATICAL ACCURACY

Mathematical accuracy is tested for all values of G_y and G_x in the interval $[-255, 255]$. Four sample test results are presented below.

Check # 1

$G_y = -160$ $G_x = -66$

$|-66| * 99 \geq |-160| * 239$ (false)

$|-66| * 99 < |-160| * 239 \&$

$|-66| * 169 > |-160| * 70$ (false)

$$|-66|*169 \leq |-160|*70 \quad (\text{true})$$

Therefore, $Dir = 90$.

Using the conventional method:

$$\tan^{-1}\left(\frac{-160}{-66}\right) = 67.583852520656^\circ.$$

Check # 2

$$Gy = -48 \quad Gx = 55$$

$$55*99 \geq |-48|*239 \quad (\text{false})$$

$$55*99 < |-48|*239 \quad \&$$

$$55*169 > |-48|*70 \quad (\text{true})$$

$$55*169 \leq |-48|*70 \quad (\text{false}).$$

Therefore, $Dir = 135$.

Using the conventional method: $\tan^{-1}\left(\frac{-48}{55}\right) =$
 $-41.1120904^\circ.$

Check # 3

$$Gy = -19 \quad Gx = -46$$

$$|-46|*99 \geq |-19|*239 \quad (\text{true})$$

$$|-46|*99 < |-19|*239 \quad \&$$

$$|-46|*169 > |-19|*70 \quad (\text{false})$$

$$|-46|*169 \leq |-19|*70 \quad (\text{false})$$

Therefore, $Dir = 0$.

Using the conventional method: $\tan^{-1}\left(\frac{-19}{-46}\right) =$
 $22.442753365294^\circ.$

Check # 4

$$Gy = 19 \quad Gx = 45$$

$$|45|*99 \geq |19|*239 \quad (\text{false})$$

$$|45|*99 < |19|*239 \quad \&$$

$$|45|*169 > |19|*70 \quad (\text{true})$$

$$|45|*169 \leq |19|*70 \quad (\text{false}).$$

Therefore, $Dir = 45$.

Using the conventional method: $\tan^{-1}\left(\frac{-19}{45}\right) =$
 $22.890551656248^\circ.$

Accuracy tests using the entire range of values in $[-255;255]$ provide the data:

- 1) Total calculated results: 261121
- 2) Total results different from 0: 260100
- 3) Total results equal to 0: 1021
- 4) Distribution of non-zero results:
 - direction 0: 65025
 - direction 45: 65025
 - direction 90: 65025
 - direction 135: 65025.

Thus it is proved that the fractions $\frac{99}{239}$ and $\frac{169}{70}$ are accurately calculated and the algorithm guarantees total accuracy.

5. EXPLORING $F_{\max}(\tan^{-1}Int)$ AND $nTclk_{\min}(\tan^{-1}Int)$ IN FPGA

Exploration methodology:

- The algorithm is implemented using all values in $[-255;255]$.

The obtained results are in Table 2.

Test results prove the functional capabilities of the proposed algorithm:

- Total mathematical accuracy
- $F_{\max}(\tan^{-1}Int) > F_{\max}(mem)$ for all values of Gy and Gx

Table 2. Results for $F_{\max}(\tan^{-1}Int)$ and $nTclk_{\min}(\tan^{-1}Int)$

FPGA family	$F_{\max}(\tan^{-1}New)$ (in MHz)	$nTclk(\tan^{-1}New)$
Cyclone	179	3
Cyclone II	259	3
Cyclone III	331	3
Cyclone IV	334	3
Cyclone V	337	3
Stratix	313	3
Stratix II	428	3
Stratix III	534	3
Stratix IV	538	3
Stratix V	540	3

- $nTclk(\tan^{-1}Int) = const = 3$ under all test conditions.

The input data widths ≤ 8 bits for both the numerator and denominator in the reference points $\frac{99}{239}$ and $\frac{169}{70}$. Because image pixel is within $[0,2^8-1]$,

for Cyclone II-V and Stratix I-V, $F_{\max}(\tan^{-1} Int)$ is defined by the maximum operating frequency of 9x9 hard multiplier. For Cyclone, $F_{\max}(\tan^{-1} Int)$ is defined by the maximum operating frequency of 8x8 logic elements based multiplier.

6. CONCLUSION

This paper presents an integer inverse tangent algorithm. Its application is focused on computing gradient direction in FPGA based edge detection which targets ultimate execution speed. The designed algorithm is explored for mathematical accuracy, maximum operating frequency and minimum number of clock cycles in ten Intel (Altera) FPGA families.

References

- [1] A. Ukil, V. H. Shah, and B. Deck, "Fast computation of arctangent functions for embedded applications: A comparative analysis", *2011 IEEE International Symposium on Industrial Electronics*, 2011, pp. 1206-1211
- [2] F. De Dinechin and M. Istoan, "Hardware Implementations of Fixed-Point Atan2", *2015 IEEE 22nd Symposium on Computer Arithmetic*, 2015, pp. 34-41
- [3] Kung, Y.-S., Wu, M.-K., Linh Bui Thi and, H., Jung, T.-H., Lee, F.-C., and Chen, W.-C., "FPGA-based hardware implementation of arctangent and arccosine functions for the inverse kinematics of robot manipulator", *Engineering Computations*, Vol. 31 No. 8, 2014, pp. 1679-1690
- [4] Luca Pilato, Luca Fanucci, and Sergio Saponara, "Real-Time and High-Accuracy Arctangent Computation Using CORDIC and Fast Magnitude Estimation", *Electronics*, 2017, pp. 6-22
- [5] M. Saber, Y. Jitsumatsu, and T. Kohda, "A low-power implementation of arctangent function for communication applications using FPGA", *2009 Fourth International Workshop on Signal Design and its Applications in Communications*, 2009, pp. 60-63
- [6] Omar Zeyad, "Design and Implementation Hardware Architecture for Four-Quadratic Arctangent", *International Journal of Computer Applications*, Volume 176 – No.1, October 2017, pp. 10-13
- [7] P. A. Kumar, FPGA "Implementation of the Trigonometric Functions Using the CORDIC Algorithm", *2019 5th International Conference on Advanced Computing & Communication Systems (ICACCS)*, 2019, pp. 894-900
- [8] Roberto Gutierrez and Javier Valls, "Low-power fpga-implementation of atan (y/x) using look-up table methods for communication applications", *Journal of Signal Processing Systems*, Volume 56, Issue 1, July 2009, pp. 25–33
- [9] R. Gutierrez and J. Valls, "Implementation on FPGA of a LUT-Based atan(Y/X) Operator Suitable for Synchronization Algorithms", *2007 International Conference on Field Programmable Logic and Applications*, 2007, pp. 472-475
- [10] R. Gutierrez, V. Torres, and J. Valls, "FPGA-implementation of atan(Y/X) based on logarithmic transformation and LUT-based techniques", *Journal of Systems Architecture*, vol. 56, 2010
- [11] S. Nandi, S. Prasad, C. M. Ananda, and S. S. Rekha, "Fixed point implementation of trigonometric function using Taylor's series and error characterization", *2016 International Conference on Advances in Computing, Communications and Informatics (ICACCI)*, 2016, pp. 442-446
- [12] S. Rajan, S. Wang, and R. Inkol, "Efficient Approximations for the Four-Quadrant Arctangent Function", *2006 Canadian Conference on Electrical and Computer Engineering. IEEE*, 2006

DEVELOPMENT OF MODELS FOR SPEECH RECOGNITION AND NATURAL LANGUAGE UNDERSTANDING USING IOT MODULES WITH PARALLEL ARCHITECTURES

Snezhana Pleshkova, Aleksander Bekyarski

Snezana Pleshkova, Technical University of Sofia, Faculty of Telecommunication, Sofia 1000 8, Kl. Ohridski blvd,
E-mail: snegpl@tu-sofia.bg

Aleksander Bekyarski, Technical University of Sofia, Faculty of Telecommunication,
Sofia 1000 8, Kl. Ohridski blvd,
E-mail: aabbv@tu-sofia.bg

Abstract

Speech recognition is one of the main methods by which artificial intelligence models a person's ability to perceive and communicate through speech. In order to achieve in speech recognition the human ability to perceive and understand speech, it is necessary to improve the already existing and achieved in practical use methods and algorithms for speech recognition and natural languages understanding. This can be done by creating pre-designed models with established accuracy to be used in various specific practical implementations of speech recognition applications. The purpose of this article is to use such predefined models and embed them in modules of Internet of Things (IoT), which have a parallel architecture and would allow real-time speech recognition.

Keywords – Speech recognition models, Parallel IoT architecture, Natural languages understanding.

1. INTRODUCTION

There are many years and many researches in area of speech recognition, which are founded the principles and the basis of the methods and algorithms for speech recognition [1]. But the real practical usage of these, developed recently methods and algorithms, is realized now with the wide spread applications of artificial intelligence in many areas of human live [2]. The aims to modelling in artificial intelligence the human speech perception and understanding ability can be satisfied using the existing and improving speech recognition methods and algorithms. One of the promising way for improving the speech recognition is to prepare the predefined speech recognition models, using them in different speech recognition applications and combining them with the achievements in area of natural languages understanding [3]. Therefore, the goal of this article is to apply some of the developed predefined speech recognition models and embedded them in modules of internet of things (IoT). It is proposed also in this article to apply internet of things (IoT) modules with parallel architecture to achieve the real time work of speech recognition and natural language understanding embedding in them the proposed and developed speech recognition models. This proposition is in accordance that the internet of things (IoT) modules with parallel

architecture are software compatible with almost of the existing predefined speech recognition models. Therefore, in the next section of this article are presented and described in details the developed speech recognition models, the choice of the internet of things (IoT) modules with parallel architecture for embedding in them the developed speech recognition models and natural language understanding.

2. DEVELOPMENT OF MODELS FOR SPEECH RECOGNITION SUITABLE TO IMPLEMENT IN IOT MODULES

There is a lot of predefined models for speech recognition [4], from which can to develop the desired model, according to concrete specifications of each speech recognition application. In general sense speech recognition models are the important parts necessary to exist in each block schemas and algorithms for speech recognition, as it is shown in Fig. 1.

The speech recognition models in Fig.1 are defined as separated acoustic, language and speech processing models, but they are intended to work together in algorithms for speech recognition. In acoustic model are included the specific characteristics of speech, i.e. the acoustic model contain the typical speech features, according to human

speech production, The language model include the necessary linguistic features of the specific natural language for which speech recognition is performed. Both, defined as acoustic and language models are necessary and are combined for using in speech processing model. As main input of this model are used usually the preliminary calculated speech features from the speech source. On the additional input to the speech processing model are submitted the data from acoustic and language models. If the speech recognition is performed only for the recognition of isolated words, the language modes is not obligatory, but for recognition the sentences of speech the language modes must exist. It can therefore be argued that the recognition process is the most important and therefore it is the subject of development in this article.

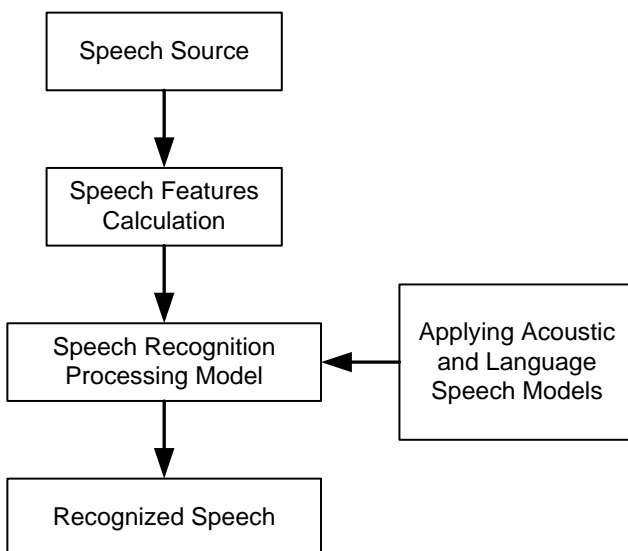


Fig.1. General view of typical block schema of speech recognition

On Fig. 2 is presented the proposed speech recognition processing model, based on the presented in Fig. 1 general view of typical block schema of speech recognition. The schema begin with speech source and speech features calculation chosen as Mel Frequency Cepstral Coefficients (MFCCs) [5]. The blocks of proposed speech recognition processing model blocks, Block 0, Block 1, Block 2 Block N and Block N+1, are surrounded by a dotted line in Fig. 2. Block 0 is the first block in speech processing model. It serves as a liaison with the Mel Features Calculation block, from which are input to the speech processing model the calculated MFCCs speech model, from which features. Block N+1 is the last block in speech processing model.

From this Block N+1 are output the results of recognized speech to the corresponding block, as it is shown in Fig. 2. The remaining blocks Block 1, Block 2 Block N are the main part of the proposed speech recognition processing model. All of the blocks, Block 0, Block 1, Block 2 Block N and Block N+1, included the similar actions as 1D Convolution, Batch Normalization, Rectified Linear Unit (ReLU), but their size and other characteristics are or can be chosen different for each of the blocks. The kernels in 1D Convolution are with k length, which is with different values for each of the blocks. The sequence of blocks 0, 1, 2 ... N, N+1 represent the layers of deep learning neural network. The activation function of each layer of neural network is chosen to be realized as Rectified Linear Unit (ReLU). It is added in each of the blocks 0, 1, 2 ... N, N+1 the Batch Normalization function to improve the learning speed of neural network and to provide regularization, avoiding overfitting. Each of the blocks 1, 2 N include L Sub blocks. The number of output channels of all sub blocks in each of the blocks 1, 2 N are equal. The input and output of each of the blocks 1, 2 N are connected via residual connection including the summing unit, as it is shown in Fig. 2.

The architecture of the sequence of sub blocks in each of the blocks 1, 2 N is the same and in presented in Fig. 3 only for a given block i from all blocks 1, 2 N. It is seen from Fig. 3, that the input and output of the block i are connected to the corresponding output and input of the block $i-1$ and $i+1$. Each sub block include the same actions 1D Convolution, Batch Normalization, Rectified Linear Unit (ReLU), as it is presented for each of the blocks 1, 2 N in Fig. 2. On the detailed presentation in Fig. 3, at the output of each sub block, after Rectified Linear Unit (ReLU), is included the action dropout. The dropout operation is used to prevent overfitting in deep neural networks at the stage of learning. Also in Fig. 3 is presented more precise the residual connection, shown briefly in Fig. 2. It is seen from Fig. 3 that the residual connection is directly between input of block i and the last sub block, but in residual connection are included 1D Convolution and Batch Normalization. Also the Rectified Linear Unit (ReLU) and Dropout in the last sub block are after summing unit.

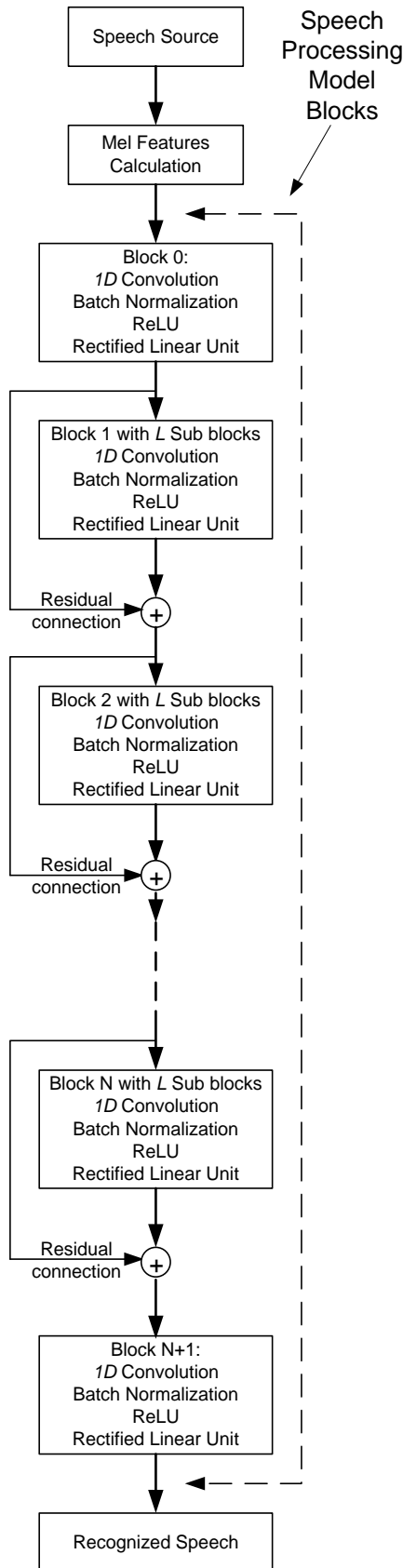


Fig. 2. Speech recognition processing model

The described above residual connection with included 1D Convolution is used in deep learning neural networks to take in account the different number of input and output channels and then pass the result through Batch Normalization.

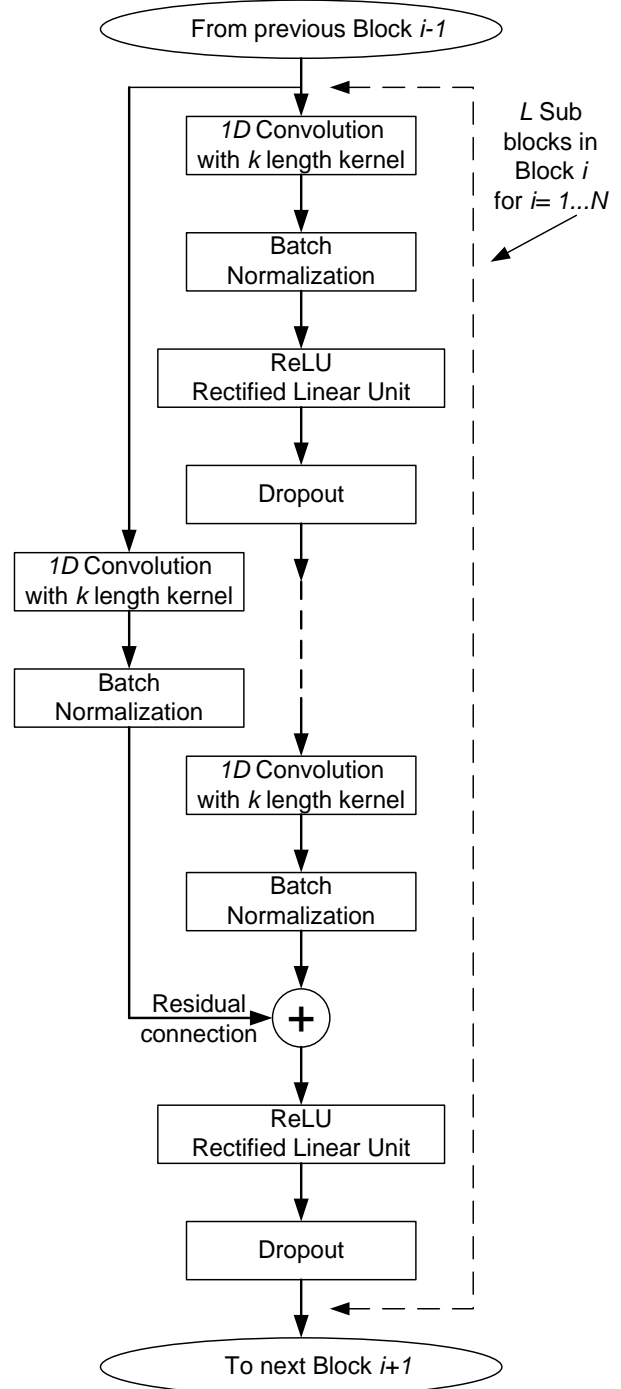


Fig. 3. Detailed schema presentation of the sub blocks in each of the blocks 1, 2 N

3. IMPLEMENTATION OF THE PROPOSED SPEECH RECOGNITION MODEL TO BE EMBEDDED IN IOT MODULE WITH PARALLEL ARCHITECTURE

The proposed and described above speech recognition model is tested as embedded in internet of things (IoT) module. It is necessary to satisfy the requirements of real time speech recognition, especially at applications such as natural language understanding. Therefore, it is proposed to embed

the described above speech recognition model in IoT module with parallel architecture. One of the most frequently used IoT modules in the implementation of neural networks with deep learning are IoT modules of NVIDIA [6]. In this article is proposed to use Jetson Nano IoT module shown in Fig. 4 with usually connected Keyboard, HDMI Monitor and necessary for recognizing input speech and for listen the input or recognized output speech USB Microphone and USB Speaker, respectively. In addition it is included the Internet connection to use the existing in Clouds Speech Models and Data Base of Natural Languages Understanding (NLU).

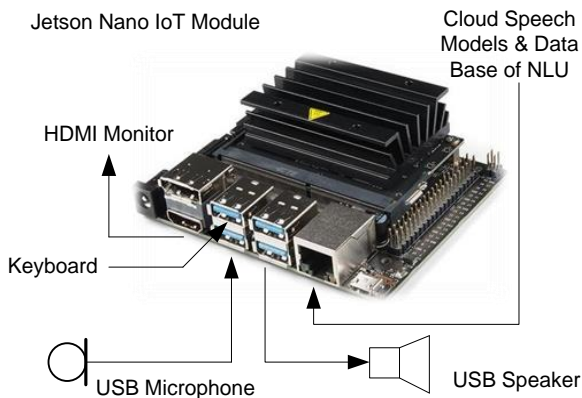


Fig. 4. Jetson Nano IoT module using to embed the proposed speech recognition model

The presented in Fig. 4 configuration of IoT module Jetson Nano is used as the base to develop the code and to test experimentally a concrete example as program application with implementation of proposed speech recognition model. For brevity, only the following important program modules of this developed as Python code are presented below to outline the main parts of proposed speech Load files to train or to test speech recognition model, presented in Fig. 2 and Fig. 3.

Speech Source Module

Load files to train or to test speech recognition

```
import librosa
```

```
import IPython.display as ipd
```

```
example_file = data_dir + '/Train1.wav'
```

```
audio, sample_rate = librosa.load(example_file)
```

```
ipd.Audio(example_file, rate=sample_rate)
```

Mell Features Calculation of

loaded files to train or to test speech recognition

```
import numpy as np
```

```
spec = np.abs(librosa.stft(audio))
```

```
spec_db = librosa.amplitude_to_db(spec, ref=np.max)
```

Train the proposed speech recognition model

using the loaded train files

```
import pytorch_lightning as pl
```

```
trainer = pl.Trainer(gpus=1, max_epochs=50)
```

```
trainer.fit(speech_model)
```

Test the proposed speech recognition model

using the loaded test files

```
import pytorch_lightning as pl
```

```
test = pl.Test(gpus=1, max_epochs=50)
```

```
test.fit(speech_model)
```

4. EXPERIMENTAL RESULTS

It can be outlined the following achieved results from experimentally tests of the proposed speech recognition model prepared as concrete example realized in program application with implementation in IoT module Jetson Nano, presented on Fig. 4. The main characteristic of the experimental speech recognition model are listed in Table 1.

TABLE I
CHARACTERISTICS OF SPEECH RECOGNITION MODEL

Number of blocks	10
Number of sub blocks in each block	5
Kernels of 1D Convolution	From 11 to 25 in Blocks 1 to 10
Output channels	From 256 to 768 in Blocks 1 to 10
Dropout	0.3

In the carried out tests are prepared the comparison with the existing in Cloud Speech Models and Data Base for Natural Language Understanding [7]. The comparison of results for speech recognition, using the developed and existing models using the same

examples of speech samples (as isolated words and sentences) and data base of natural language model are presented in Table 2.

TABLE II
COMPARISON OF THE DEVELOPED SPEECH RECOGNITION MODEL
WITH SOME EXISTING SPEECH RECOGNITION MODELS

Existing Models [7]	Comparison of precision in % of speech recognition using the developed and the existing models
Model 1	82% to 89%
Model 2	76% to 88%
Model 3	83% to 97%
Model 4	87% to 95%

5. CONCLUSION

The briefly presented in Table 2 overall comparative results for speech recognition, using the developed and existing models can be comment in the following way.

In general the results of speech recognition, using the proposed speech recognition model, are similar (but with lower 76-87 % accuracy) in comparison of the same examples of speech recognition using the existing models (88-97%). This can be explain with the following arguments:

- insufficient in-depth training of the proposed model compared to the existing ones;
- more precisely defining the parameters of the neural network with deep training for the existing speech recognition models;
- greater number of blocks, corresponding sub blocks and the number of channels in the layers of neural network with deep learning in existing speech recognition models, using in comparison.

Regardless of this differences from the existing speech recognition models, the following advan-

tages of the proposed speech recognition model can be highlighted:

- simpler scheme suitable for embedding in IoT modules with less complexity of parallel architecture, like IoT module Jetson Nano;
- preference for use in simple practical applications for speech recognizing a limited number of words and sentences and from a specific natural language for examples mobile robots or other devices, using limited words and sentences as speech commands in voice control.

ACKNOWLEDGMENTS

The authors would like to thank the Research and Development Sector at the Technical University of Sofia for the financial support.

References

- [1] A. Graves and J. Schmidhuber, "Framewise phoneme classification with bidirectional lstm and other neural network architectures," *Neural Networks*, vol. 18, pp. 602–610, 2005.
- [2] By Janna Anderson, Lee Rainie and Alex Luchsinger, "Artificial Intelligence and the Future of Humans", Pew Research Center, December, 2018.
- [3] P. Liang, "Natural Language Understanding: Foundations and State-of-the-Art", *ICML*, July 6, 2015.
- [4] D. Wang, X. Wang and S. Lv, "An Overview of End-to-End Automatic Speech Recognition", *Symmetry* 2019, 11.
- [5] H. Perez-Meana and E. Escamilla-Hernandez, "Speaker recognition using Mel Frequency Cepstral Coefficients (MFCC) and Vector quantization (VQ) techniques", *CO-NIELECOMP*, 22nd International Conference on Electrical Communications and Computers, 2012.
- [6] Jetson Nano Developer Kit, <https://developer.nvidia.com/jetson-nano-developer-kit>
- [7] NVIDIA Cloud Computing. <https://www.nvidia.com/en-us/data-center/gpu-cloud-computing>

AUTHOR INDEX

AMPILOVA, N.	8
ANTONOV, S.	1,5
BEKYARSKI, A.	35
GHVEDASHVILI, G.	21
JELADZE, V.	21
KADOMSKIJ, A.	18
KROMICHEV, D.	25,30
KURTSIKIDZE, M.	21
NOZADZE, T.	21
PLESHKOVA, S..	35
SHEIRETSKI, K.	1,5
SOLOVIEV, I.	13